Fabrication of Ferroelectric Thin Films using 355nm Pulsed Laser

By

Muhammad Waqas

DEPARTMENT OF PHYSICS

QUAID-I-AZAM UNIVERSITY

ISLAMABAD, PAKISTAN

2021-2023


بسم الله الرحمن الرحيم

This work is submitted as a dissertation

In partial fulfillment of the requirement for the degree of

MASTER OF PHILOSOPHY

IN

PHYSICS

To The

Department of Physics

Quaid-I-Azam University

Islamabad, Pakistan

2023

CERTIFICATE

This is to certify that the experimental work in this dissertation has been carried out by ***Mr. Muhammad Waqas*** under my supervision in the Superconductivity and Magnetism Lab, Department of Physics, Quaid-I-Azam University, Islamabad, Pakistan.

Supervisor:

Prof. Dr. Arif Mumtaz

Department of Physics

Quaid-I-Azam University

Islamabad, Pakistan.

Submitted Through:

Prof. Dr. Kashif sabeeh

Chairman

Department of Physics

Quaid-I-Azam University

Islamabad, Pakistan.

DEDICATION

To

My Ammi and Baba

And

My Brothers

ACKNOWLEDGEMENTS

All praises and thanks to Allah Almighty, the All-Knowing, the All-Seeing, the All-Hearing, the All-Aware, the All-forgiving, the All-praise-Worthy, who granted me the courage, patience, intelligence, health, and consistency to be able to pursue my dreams. All my achievements, from drawing my first breath to the submission of this dissertation.

I feel great pleasure in expressing my deepest regard and respect for my supervisor **Prof. Dr. Arif Mumtaz**. He has been a great mentor throughout this expedition. His constant guidance, encouragement, patience, kindness, and forbearance played a vital role in accomplishing this task. His encouraging discussions enabled me to broaden and improve my capabilities in Physics. I also want to thank **Prof. Dr. Raheel Ali,** who was very helpful and kind throughout my journey.

My heartfelt love and thanks to my dearest **Ammi** and **Baba** whose ever-present love, kindness, support, upbringing, faith, and encouragement has made me the person I am today. My profound thanks to my loving and caring brothers **Ahmad Ali, Abdullah,** and my sister-in-law **Mehwish**, who helped and encouraged me throughout my studies.

Lastly, I would like to acknowledge all my friends who are always there for me through every thick and thin and whose friendship I cherish the most.

Muhammad Waqas

Abstract

Barium titanate (BTO) is an interesting/well-known ferroelectric material due to the existence of ferroelectric properties at room temperature, which makes it very useful for potential devices. Already prepared pure BTO pellets used to synthesis Thin Films. Pulsed Laser Deposition (PLD) method is used to synthesis Thin Films, in this work 355nm Pulsed Laser is used and the aim of this is to check how this range of laser effect the properties of the Thin Film prepared at different temperatures. The structure of the prepared films is investigated using XRD analysis. For the study of morphology of the films SEM and AFM analysis were carried out. Specifically, SEM analysis is for how the films look like and for grain size analysis. AFM analysis is for roughness of the films, the height and phase images, 3-D images, and line measurement were carried out to investigate the roughness of the films. Optical properties and bandgap studies of all the pure BTO have been carried, these results were found to be consistent and within the spectral range of 2.2 eV to 3.6 eV. Increase in the synthesis temperature of the thin films resulted in the decrease of band gap and increase smoothness of the films.

List of Figures

List of Tables

Table of Contents

Chapter-1 Introduction and Background

In recent years, scientists have become really interested in these super tiny materials called nanomaterials. They are particles that are incredibly small, even smaller than what we can see with our eyes. People are studying them in different areas like chemistry, physics, biology, and engineering particularly in condensed matter physics and materials science. They exhibit a wide range of fascinating functionalities, including high-temperature superconductivity [1], ferroelectricity [2], magnetism [3], colossal magnetoresistance [4], piezoelectric [5] and recently the multiferroic properties [3]. One thing that makes these tiny particles special is that they have a lot of surface area compared to their size (<100 nm). It's like they have many tiny spots on their surfaces.

This is really cool because it means they can do special things and have better properties for various uses. For example, they can be used in catalysts to make chemical reactions happen more efficiently. In electronics, their unique electronic and optical properties make them useful for making better devices. They are even used in medicine for delivering medicines to our bodies more effectively. Within nanomaterials, there's a specific type called ferroelectric thin films, and scientists are really excited about them. These films are extremely thin and don't weigh much. Because of their unique properties, they can be used in many things. They are great for making high dielectric capacitors, which store and release electric charge in electronic devices. These capacitors are essential for many gadgets, and using ferroelectric thin films can make these devices smaller and more efficient. Scientists are also studying these thin films for non-volatile memories, which are storage devices that keep information even when they are turned off. The low amount of energy needed to switch them on and off is a really good feature for these memories, and ferroelectric thin films seem to have that capability. They are also being explored for infrared sensors and electro-optics devices, where they can help these devices perform better [6].

One of the most popular materials in the ferroelectric thin film group is called perovskite $BaTiO_3$. It's getting a lot of attention because it has some amazing properties. For example, it can store a lot of electric charge, making it really useful for advanced memory technologies. It also doesn't waste as much energy as heat, which is great for energy efficiency. It doesn't let electricity leak out easily either, so the charge can stay in it for a long time. The way it behaves at different temperatures can also be controlled depending on its composition. Because these properties are so useful and promising, scientists have been studying how to make nanomaterials and thin films using perovskite $BaTiO_3$ for many years [7]. They are really excited to see what new and exciting things they can do with these tiny materials in the future.

1.1 Materials

Eventually, interest in determining the current and voltage characteristics of dielectric thin films. Electronic conductivity refers to the conductivity that results from the movement of electrons or positive holes. Ionic conductivity refers to the conductivity caused by the movement of ions. n-type conductivity and p-type conductivity are both terms used to describe the conductivity of electrons and holes, respectively. The electrical conductivity of metals increases as the number of electrons available for conduction increases, resulting in an increase in electrical conductivity. Ions are unavailable for conduction in pure ionic solids, making them insulators in their solid state. Electrical conductivity rises because of crystal defects. Solids have a wide variety of electrical conductivities ranging from 10^{-20} to 10^{7} ohm^{-1} m^{-1}. Based on their conductivities, solids can be categorized into three categories. Band theory has been used to explain the difference in conductivity between conductors, insulators, and semiconductors (Dielectrics) [8].

1.2 Optical property

The energy gap in a semiconductor can be measured in several ways. The optical properties of crystal are one of the most important sources of information. When the frequency of the incident photon becomes large enough for ω_g to exceed the energy gap, then, there will be an abrupt increase in the absorption of incident radiation. The threshold of continuous optical absorption at frequency ω_g determines the band gap $E = \hbar\omega_g$.

Thus identify the type of process that is dominant (indirect, direct, allowed, forbidden. etc.) at the band edge. However, if we are interested in the optical properties of a semiconductor over a wide energy range, then we want to treat all bands and transitions within a few eV from the Fermi level on an equal footing. Away from the band edge, the absorption coefficients become too high for the absorption technique to be useful and reflectivity measurements are made instead. Experimentally it is most convenient to carry out reflectivity measurements at normal incidence.

1.2.1 Energy band gap

The band gap is the difference in the energy between the lowest point in the conduction band and the highest point of the valance band. The lowest point in the conduction band is called

the conduction band edge, the highest point in the valance band is called the valence band edge. There are two types of band gaps which are as follows:

1.2.1.1 Direct band gap

If the conduction band minimum occurs in the same point in the k-space as the valance band maximum, then the energy gap can be directly determined from the optical threshold and the band gap is called the direct energy band gap Figure 1:1 (a). The semiconductors having such bands are called direct-gap semiconductors.

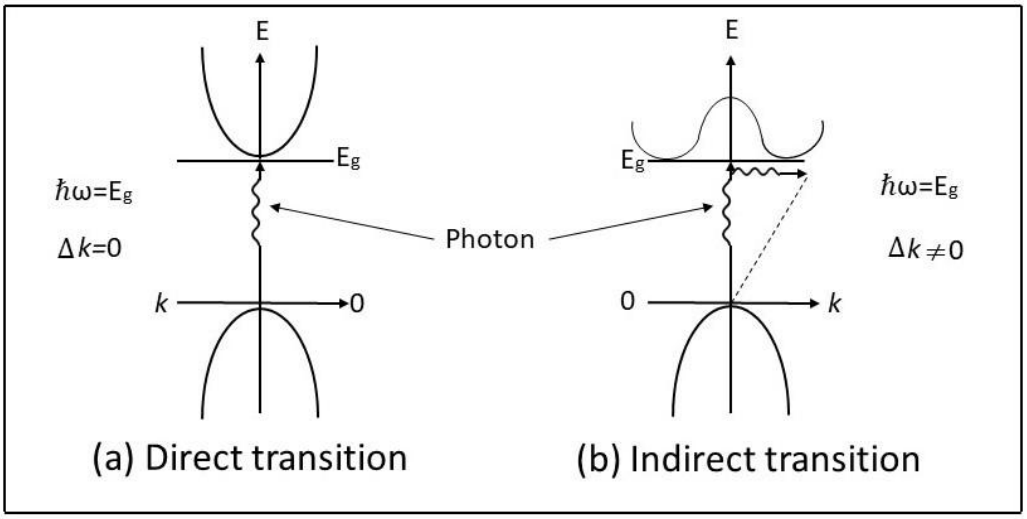

Figure 1:1: The band gap by photon absorption (a) direct band gap, (b) indirect band gap

1.2.1.2 Indirect band gap

If the conduction band minimum and valance band maximum occur at different points in k-space then for crystal momentum to be conserved a phonon must also participate in the process, which is then known as an "indirect transition" Figure 1:1 (b) Since the phonon will supply not only the missing crystal momentum $\hbar k$, but also energy $\hbar\omega$, the photon energy at the optical threshold will be less than E_g by an amount of the order $\hbar\omega$. This is typically a few hundredths of an electron's volt. The band gap in this case is called the indirect band gap. The semiconductors having such a band are called indirect-gap semiconductors.

1.3 Energy Bands of Solids

1.3.1 Conductors

Metals are solids with conductivities between 10^4 and 10^7 ohm^{-1} m^{-1}. The conduction band and valance band are very close to each other, So the valence electron can easily move into the conduction band [9]. Examples, Silver, Gold, Copper.

1.3.2 Insulators

Insulators are solid materials in which the gap between the conduction band and valance band is larger [9]. Insulator's conductivities range in between 10^{-10} and 10^{-20} ohm^{-1} m^{-1}. Examples, Wood, Glass, Paper.

1.3.3 Semiconductors and Dielectrics

Solids that exhibit electrical conductivity between 10^{-6} and 10^4 ohm^{-1} m^{-1} are called semiconductors. Semiconductors and dielectrics are the solid materials with completely empty conduction band above the filled valance band [9]. The forbidden energy gap in dielectric materials is comparatively larger than the semiconductor materials. The electrons are strongly bounded in the valance band, but they get polarized in the presence of the external field. In the semiconductor the forbidden energy gap is less than 2eV, and in dielectric substances, the forbidden gap is larger than 3eV as shown in figure 1:2.

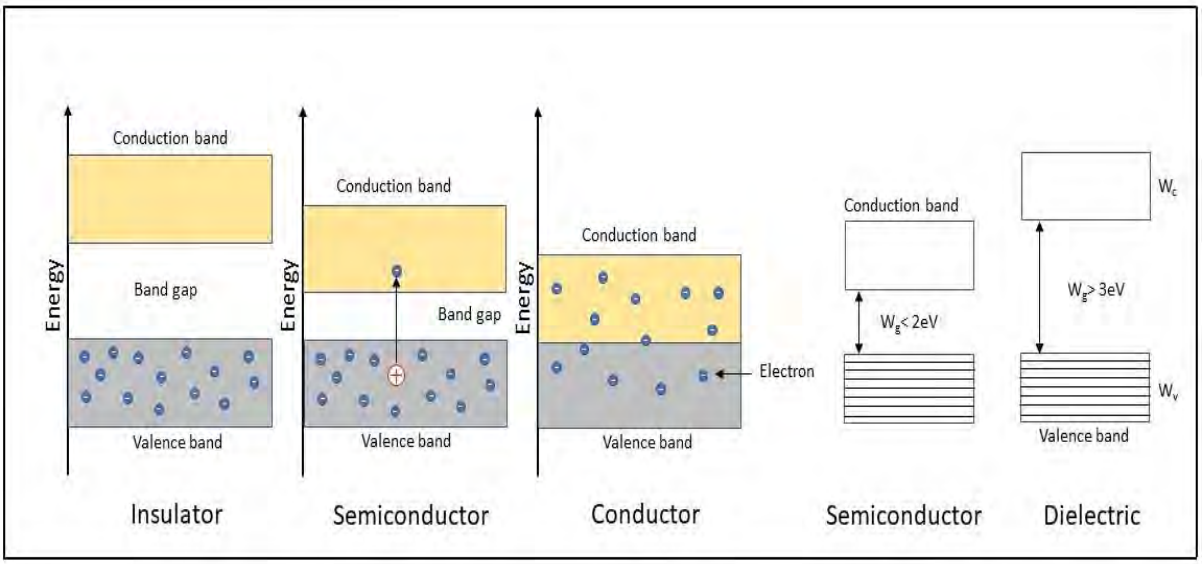

Figure 1:2: Band digram of insulator, semiconductor, conductor, and band comparison of semiconductor and dielectric.

1.4 Polarization

When an electric field is applied to dielectric materials, they become polarized. The net polarization is defined as the induced dipole moment divided by the volume unit as given by

$$\vec{P} = \frac{\Delta \vec{p}}{\Delta V}$$

Where $\vec{p}$ is dipole moment, V is net volume and $\vec{P}$ is total polarization. Another way to define electric polarization is the rearrangement of charges within a material resulting from the influence of an external electric field.

1.4.1 Types of Polarization

Dielectric materials exhibit four primary forms of electric polarization.

1.4.1.1 Electronic Polarization

When an external electric field is absent, the positively charged nucleus and negatively charged electronic cloud of an atom have the same center. However, when an external electric field is applied the electronic cloud shifts slightly from its original position which results in one end of the atom becoming positively charged, and the other end becoming negatively charged

[10]. This process is induced by the external electric field and referred to as electronic polarization as shown in Figure 1:3. It typically takes about 10-15 seconds to activate as can be seen in Figure 1:3 [11]. Electronic polarization mostly occurs at high frequencies of electric field, and it can be observed in all types of atoms and molecules.

$$P_e = \alpha_e E$$

Where E is external electric field,

$$\alpha_e = 4\pi\mathcal{E}_o R^3 = 3\mathcal{E}_o V_{atm}$$

Where $V_{atm} = \frac{4}{3}\pi R^3$,

The electronic polarizability of an atom is denoted by α_e. It is the ratio of induced dipole moment in the system to the applied external electric field and is directly proportional to the volume of the electronic shell. It is independent of temperature and can be expressed in terms of the atom's radius R.

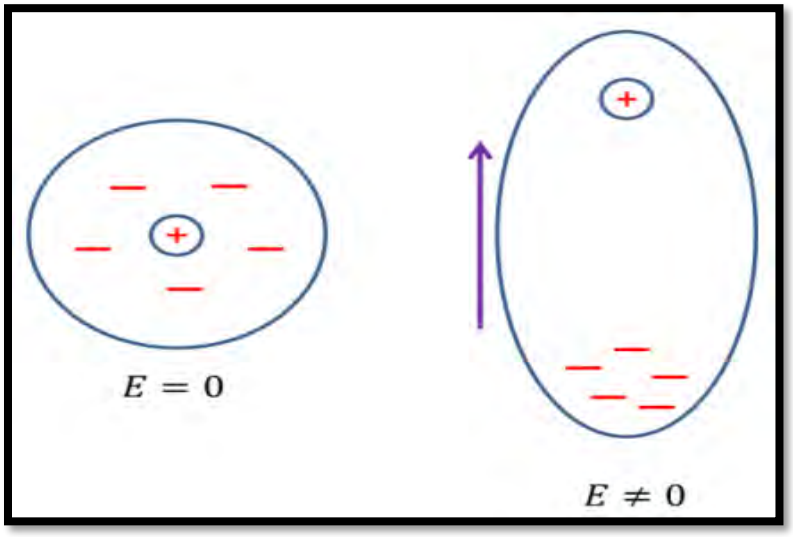

Figure 1:3: Shift of electron to center when $E \neq 0$ [10].

1.4.1.2 Ionic Polarization:

Ionic materials exhibit ionic polarization, which occurs because of the displacement of positively and negatively charged ions in opposite directions of an applied electric field as shown in Figure 1:4. Although ionic materials have dipoles and they do not possess net polarization in

the absence of a field because the dipoles of positive and negative ions cancel each other out. However, when an external field is applied. The cations and anions within the material slightly shift from their equilibrium positions and result in a net dipole moment [11]. Mathematically, this induced dipole moment is given as.

$$P_i = \alpha_i E$$

Where E represents local electric field and α_i ionic polarizability.

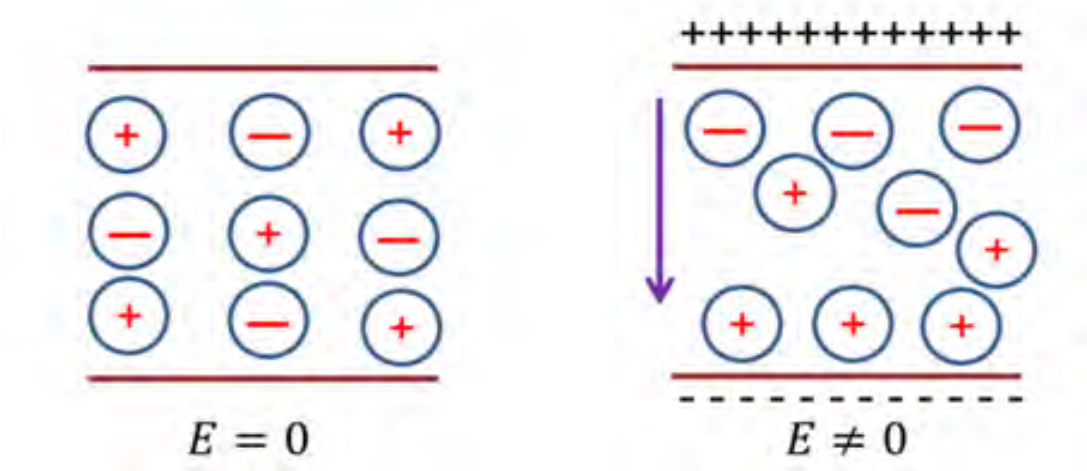

Figure 1:4: Displacement of ions when $E \neq 0$ *[10]*.

1.4.1.3 Orientational Polarization:

Polar molecules such as H_2O and HCl, exhibit orientation polarization because of their permanent dipole moments. In the absence of an applied electric field, these polar molecules have zero net polarization because their permanent dipoles are randomly oriented in every direction which effectively cancelling each other out and thus resulting in a zero average dipole moment [12]. When an electric field is applied, the dipole moments within a material become oriented in the same direction as the applied field. This results in the causing of orientational polarization within the material as shown in Figure 1:5. The average dipole moment can be expressed as follows.

$$\boldsymbol{P_o = \alpha_o E}$$

Where $\alpha_o = \frac{p^2}{3KBT}$,

E refers to external electric field and α_o is the orientational polarizability respectively. The above equation shows that it is temperature dependent unlike electronic and ionic polarization.

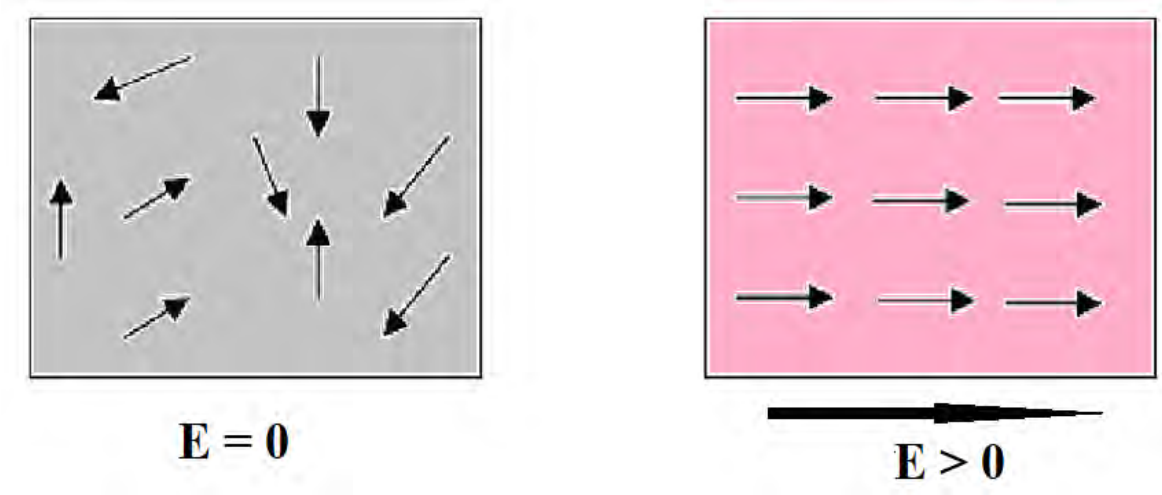

Figure 1:5: Orientational polarization [13].

1.4.1.4 Space charge Polarization

A form of polarization that arises due to the accumulation of charge carriers at interfaces between different regions of a single crystal or at the boundaries between grains in polycrystalline dielectric materials. This type of polarization is also referred to as interfacial polarization. This form of polarization is commonly observed in ceramics [14]. Space charge is the distribution of electric charge over a particular region of space, rather than being concentrated at specific point-like locations. Space charge polarization arises due to the presence of defect sites within the dielectric material, which cannot be eliminated. The presence of charges at grain boundaries contributes to an increase in the dielectric constant. As the temperature increases these charges participate in conduction processes, which leads to the occurrence of a phenomenon called Maxwell-Wagner relaxation in dielectrics [12]. Figure 1:6 depicts the space charge polarization and mathematically it is expressed as,

$$\boldsymbol{P_{sc} = \alpha_{sc} E}$$

Where α_{sc} represent space charge polarizability.

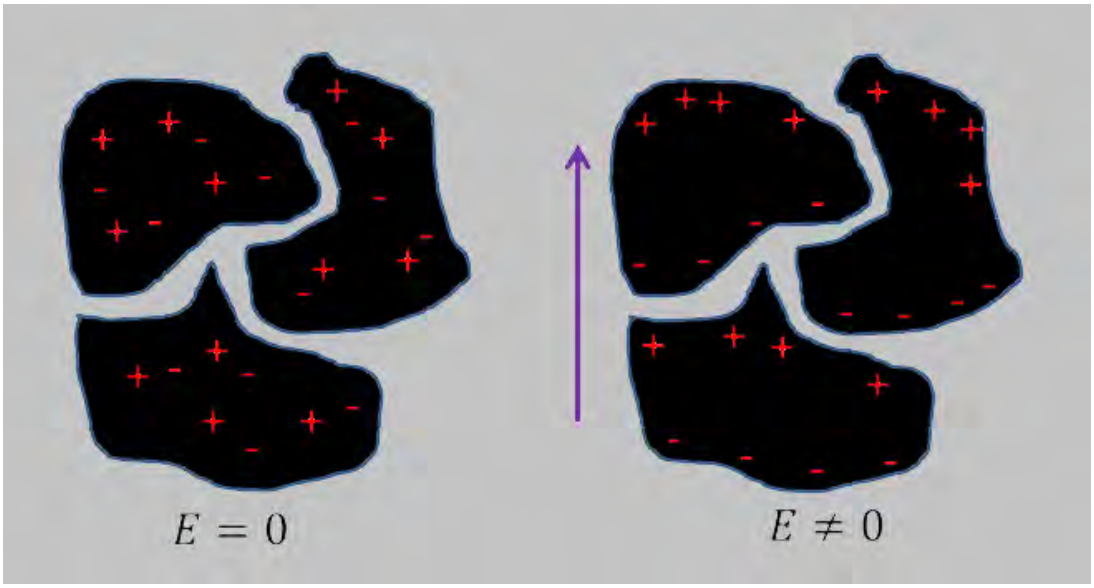

Figure 1:6: Space charge (Interfacial) Polarization *[10]*.

1.5 Classification of Materials

There are 32 different classes of crystalline materials. Out of the 32 crystal classes (i.e., point groups), 11 have a Centre of symmetry and as a result cannot exhibit polar properties. The remaining 21 are non-centrosymmetric and therefore can keep one or more polar axes. Of these, 20 classes are piezoelectric (the one leaving out being cubic class). Piezoelectric crystals possess the feature that the application of mechanical stress induces polarization, and equally, the application of an electric field yields mechanical deformation. Out of the 20 piezoelectric classes, 10 possess a unique polar axis and so are instinctively polarized, i.e., polarized when there is no applied electric field. Such crystals are called pyroelectric. Ferroelectric materials classification based on symmetry is shown in figure 1:7.

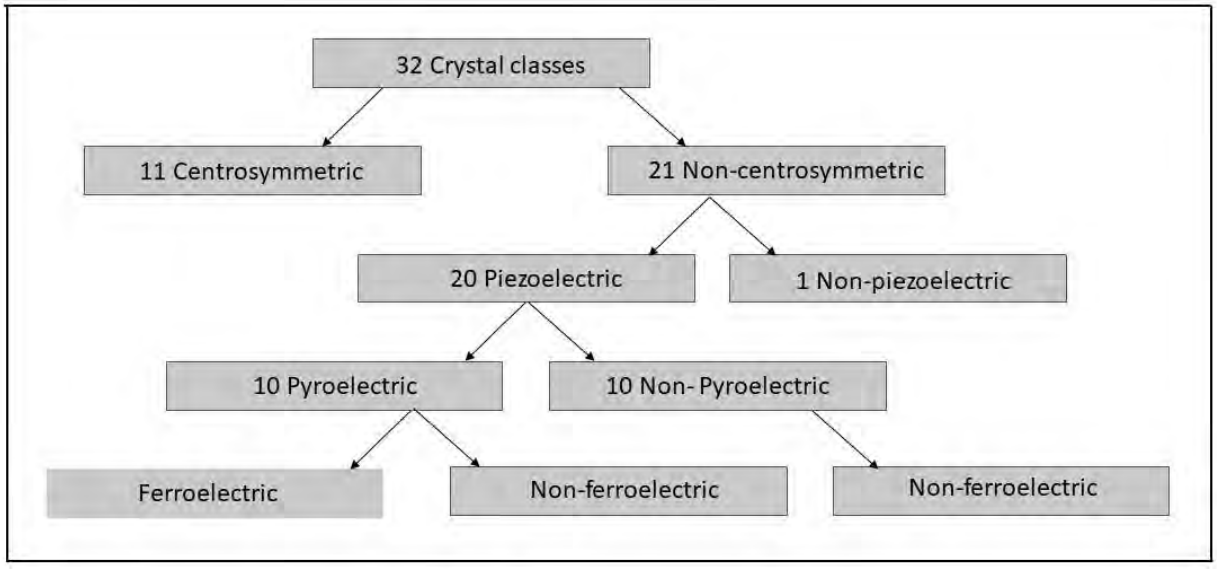

Figure 1:7: ferroelectricity classification based on symmetry consideration.

The intrinsic polarization is a function of temperature, so the natural moment in these crystals is usually achievable to observe by fluctuating the temperature, thus the name pyroelectrics. Ferroelectric crystals, a limited group of pyroelectric family, also exhibit the additional characteristic that the direction of the spontaneous polarization can be overturned (reoriented) on application of an applied electric field. Hence, every single ferroelectric is pyroelectric and piezoelectric but the entire piezoelectric are not pyroelectric and all pyroelectrics are not ferroelectric.

1.5.1 Paraelectric

Paraelectric materials are the class of dielectric that have no dipole in the absence of applied electric field. When electric field is applied, dipoles may form but that will be weak in strength and will be removed when that external electric field is removed.

1.5.2 Pyroelectrics

Pyroelectricity is from two Greek word *pyr* mean fire and electrics is electricity, so as by the name of pyroelectrics is type of material which generate a temporary voltage when they are heated and cooled.

1.5.3 Piezoelectric

Materials that exhibit piezoelectricity can generate electricity under the application of mechanical stress, or conversely, producing mechanical stress upon exposure to an applied electric field [15]. The piezoelectric effect is observed in materials possessing a non-centrosymmetric crystal structure. In centrosymmetric crystal structure, the dipoles cancel each other's effect which results in an absence of a net polarization [15]. Piezoelectric materials, such as Barium titanate ($BaTiO_3$), Lead titanate ($PbTiO_3$), and PVDF are widely used in various fields due to their ability to generate electric charge under mechanical stress or produce mechanical stress in response to an applied electric field [16]. These materials are highly valued for their functionality, which includes sensing, actuation, and biomedical applications etc. The piezoelectric effect observed in quartz is shown in Figure 1:8.

$$P = d.\mathrm{T}$$

Where P is direct piezoelectric effect, d is piezoelectric coefficient, and T is small amount of stress.

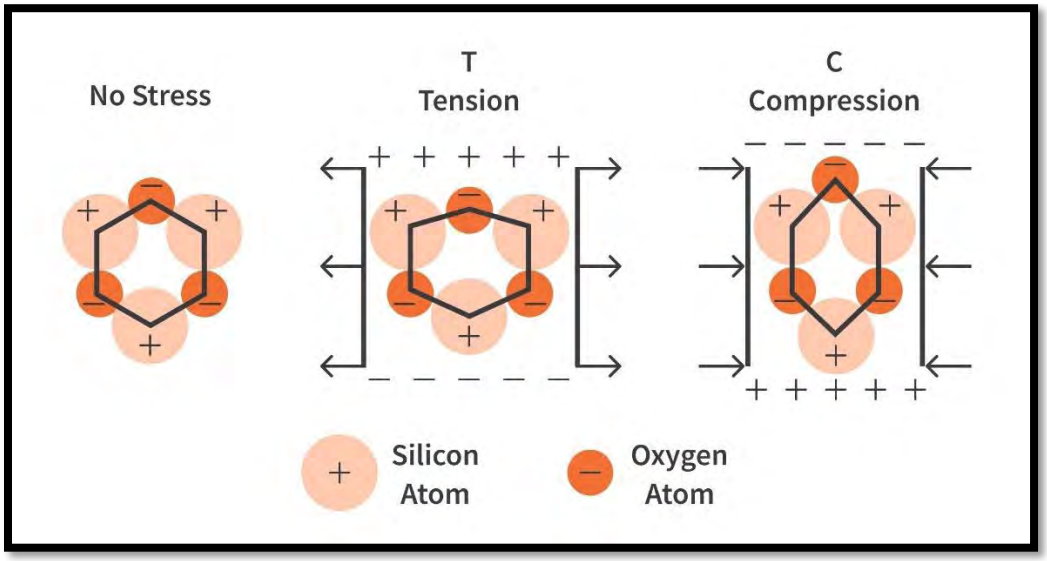

Figure 1:8: Piezoelectric effect in Quartz [17].

1.5.4 Ferroelectrics

Ferroelectrics are a special class of material which exhibit spontaneous polarization. In ferroelectric materials the direction of polarization can be switched by switching the direction of applied electric field and dipole moment of the unit cell is spontaneously aligned with its neighboring unit cells even in the absence of applied electric field. In 1921, Valasek discovered Rochelle salt, which led to the discovery of ferroelectricity and then ferroelectric materials.

1.5.4.1 Ferroelectric Domains

In ferroelectric materials, spontaneous polarization has the same probability to align in all crystallographic orientations in the absence of the external field. The region where all the dipole in the ferroelectric crystal has the same direction is called ferroelectric domain and the direction of one domain could be varied from the adjacent domain. The boundary among the two domains is named as domain wall. The width of the domain wall is usually of the order of one or two nanometers. Naturally in ferroelectric materials, the domains have random directions and will result in zero net ferroelectric polarization. In ferroelectric materials, the domains are generated to reduce the electrostatic energy produced by the depolarization of the electric field. These ferroelectric domains also diminish the strain energy which is linked with the mechanical constraint that arises during the temperature-dependent phase transition. When the spontaneous polarization is not homogeneously distributed in the material, then the phenomena of depolarization will appear. The decrease in the ferroelectric polarization at the wall of the grain is also due to the depolarization effect which resulted in the decrease in the ferroelectric response of the material. Since the depolarization filed is usually very high (of the order of 10 kV per centimeter), therefore it tends to restrict the formation of a single domain in a ferroelectric material, as a result, the domains are split into opposite ferroelectric polarization. The criteria for the prediction of domain orientation in a perfect single crystal are introduced by Fousek et al., [5]. He established three points which are: 1st – During the phase transition the structure of the material alters, and this alteration can be detected by the change in amplitude and phase of the polarization. 2nd – The domain wall of two domains having different polarization directions will be common only if two alterations in a lattice accurately resemble each other. In a tetragonal structure, the polarization in a domain can be aligned only in three mutually orthogonal crystallographic axes. Here, we have two kinds of grain boundary (wall). First, if the polarization

direction in the two domains is opposite to each other than the wall is called 180^0-wall while the domain with perpendicular polarization direction is named as 90^0-wall. The schematic diagram of the domain wall distribution is shown in Figure 1:9, where a black dotted line represents the 180^0 domain wall while a solid black line indicated the 90^0 walls in a ferroelectric material.

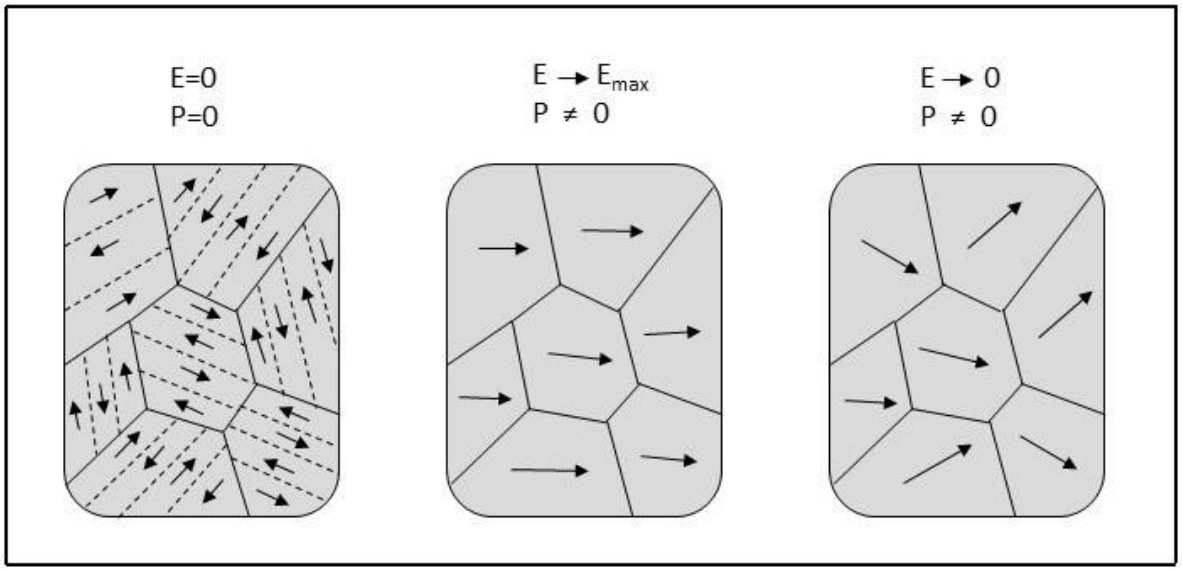

Figure 1:9: schematic representation of domains in ferroelectric materials.

1.5.4.2 Ferroelectric Hysteresis

Ferroelectric materials can be identified by the presence of a P-E loop referred to as a hysteresis loop that demonstrates a relationship between polarization (P) and the applied electric field (E). In ferroelectric materials, reversible spontaneous polarization appears with the application of an electric field. The domains begin to align in the direction of field when electric field is applied. More and more domains align in the field direction as the field strength grows, until eventually all domains are aligned, and polarization reaches its saturation state Ps as shown in figure. When the field is removed the dipole moments did not completely randomize and polarization remains. The polarization vanishes completely in ferroelectric materials when electric field is applied in opposite direction. This is identical to ferromagnetism, in which a ferromagnet can retain its magnetization after being exposed to a magnetic field. The graph

below in figure 1:10 represents a ferroelectric hysteresis loop, which is like a magnetic hysteresis loop in its fundamental structure.

A ferroelectric hysteresis loop has three important points.

1. **Electric coercivity (EC)**

   Electric coercivity is the electric field where the polarization of ferroelectric capacitor disappears.

2. **Remnant polarization (PR)**

   In Remnant polarization the polarization remains in the substance even if the electrical field is removed.

3. **Saturation polarization (PS)**

   Saturation polarization is in high electric field strength, the highest amount of polarization that can be induced in the material.

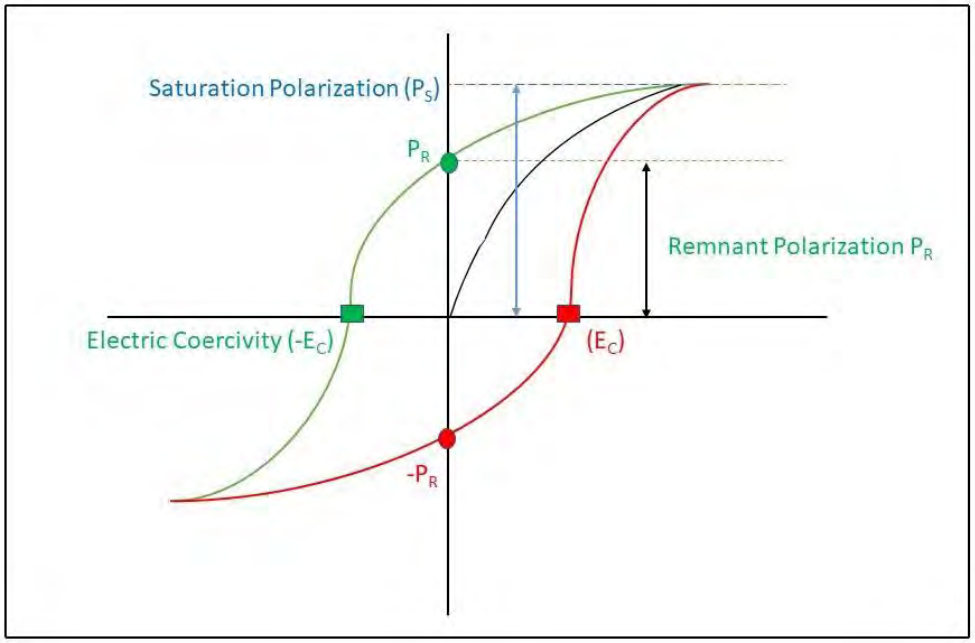

Figure 1:10: Hysteresis loop for ferrolectric materials showing complete polarization.

1.6 Type of Ferroelectrics

1.6.1 Normal Ferroelectrics

Ferroelectric materials are special because they have a built-in electric charge, and this charge stays even if we remove the electric field around them. This is called "spontaneous electric polarization." This property makes them unique and gives them some cool abilities, like having a high ability to store electric charge (called "dielectric constant") and being really good at converting pressure into electricity (called "piezoelectricity"). When the electric polarization is fixed in just one direction, we call it "normal ferroelectricity" [18]. Some examples of materials that show this behavior are barium titanate, lithium niobate, and strontium bismuth tantalate. We use these materials in different things, like capacitors (for storing electric charge), sensors (to sense things around us), and non-volatile memory devices (for long-term data storage).

In contrast, there are also other ferroelectric materials called "relaxer ferroelectric materials" that behave differently. But the ones we talked about, like barium titanate and the others, are examples of "normal ferroelectric materials" that have exciting properties for various applications in electronics and sensors.

1.6.2 Relaxer Ferroelectrics

Ferroelectric relaxer materials are special because they show something called "relaxer ferroelectricity." Unlike normal ferroelectric materials where the electric polarization is fixed in just one direction, in relaxer ferroelectric materials, this polarization changes and moves around within the material [19]. We call this movement "relaxation." This relaxation gives these materials some cool abilities, like having a high ability to store electric charge (dielectric constant) and being really good at converting pressure into electricity (piezoelectricity). One important thing about relaxing ferroelectric materials is that they can keep a strong polarization over a wide range of temperatures.

Because of these properties, we use them in various devices, like sensors (to sense things), actuators (to make things move), and memory devices (for storing information). Examples of relaxer ferroelectric materials are lead magnesium niobate-lead titanate (PMN-PT) and lead zirconate titanate (PZT). So, relaxer ferroelectric materials are a bit different from

normal ones, but they have some exciting features that make them very useful in many applications.

1.7 Ferroelectric Phase Transition

A ferroelectric phase transition is a special change that happens in a ferroelectric material at a particular temperature. When this transition occurs, the electric polarization of the material changes. This can happen because we apply an electric field to it or when the temperature changes [20]. The ferroelectric phase transition can be of two types: first-order or second order. In a first-order transition, the electric polarization suddenly changes at the transition temperature, like a quick switch. On the other hand, in a second-order transition, the electric polarization changes smoothly as the temperature changes. These phase transitions are essential because they give ferroelectric materials some very unique properties. For example, $BaTiO_3$ (BTO), they can hold a lot of electric charge (high dielectric constant) and convert pressure into electricity (high piezoelectricity). These properties are very helpful in making devices like capacitors, sensors, and memory devices that we use in many electronic applications. So, ferroelectric phase transitions are critical for creating materials with special abilities that are useful in various technologies we use in our daily lives. The phases of BTO with temperature is shown in the figure 1:11.

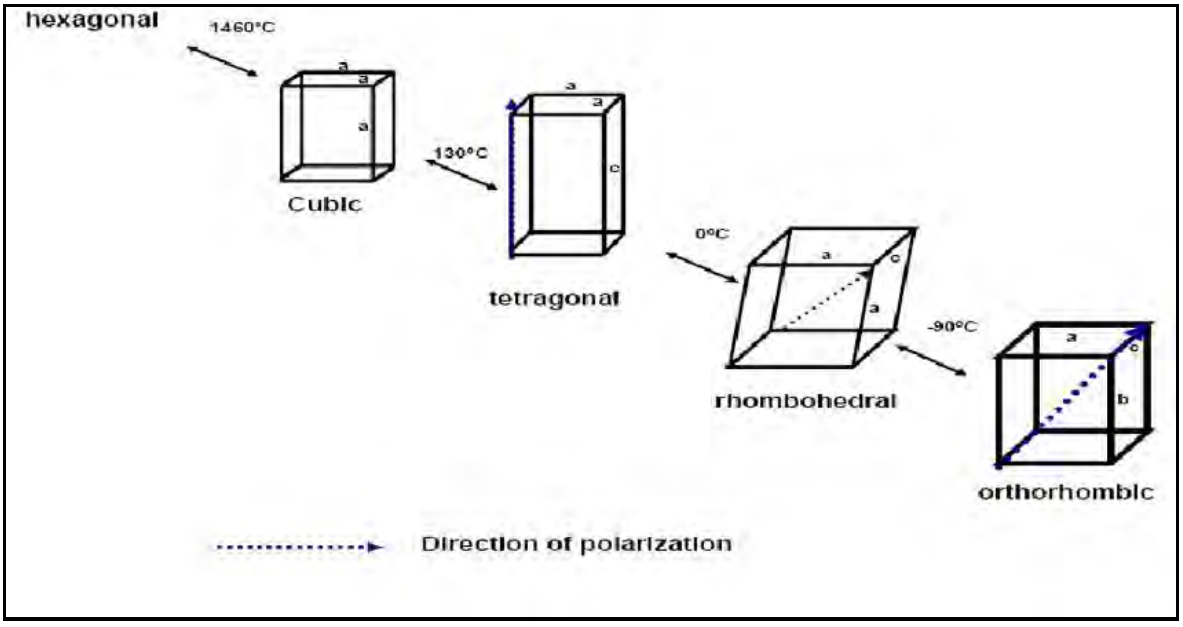

Figure 1:11: Phase diagram of BTO with temperature [21].

1.8 Perovskite structure

Perovskite materials got their name from Count Lev Alekseyevich von Perovski, who was a Russian mineralogist. Perovskites are a type of crystal that have similar properties to a specific one called $CaTiO_3$. Their chemical formula is written as ABX_3. There are two cations ('A' and 'B') located at the corners of a cube, and an anion ('X') located at the face centers as shown in figure 1: 12. The valence of an A-site cation is often between +1 and +3, whereas the valence of a B-site cation is typically between +3 and +6. In most perovskites, the ionic radius of the A-site cation is higher than that of the B-site atoms, whereas the anion 'X' is predominantly a fluorine or oxygen ion. Due to the existence of interaction between spin, charge, and orbits in perovskites, they have received considerable interest due to their electric, magnetic, transport, and multiferroic properties [22].

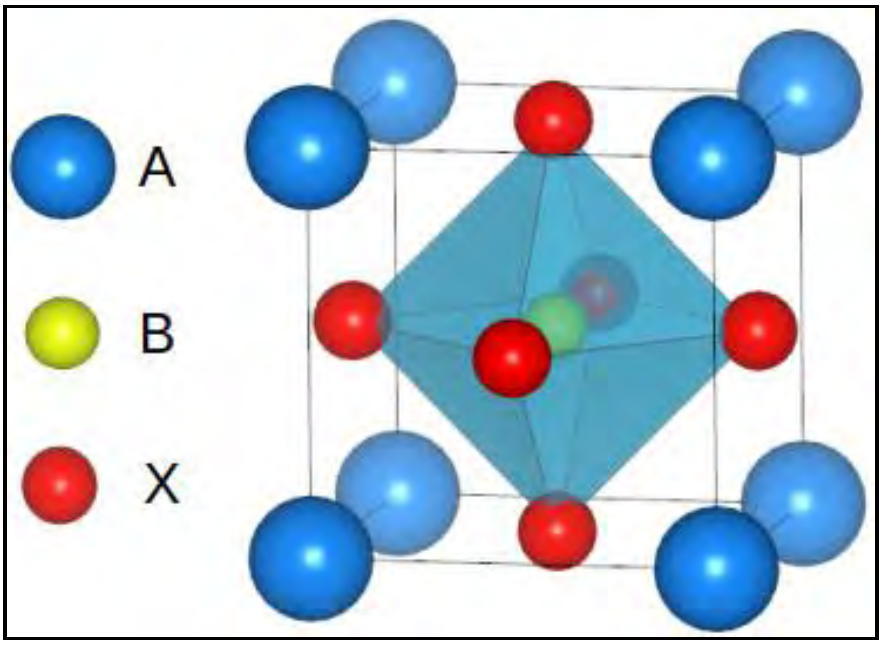

Figure 1:12: ABX_3 perovskite unit cell.

1.9 Barium Titanate (BaTiO3)

The chemical formula of barium titanate is $BaTiO_3$ and has a perovskite structure (with A = Ba and B = Ti of ABO; type perovskite material). It attracts much attention because of its high tenability, high dielectric permittivity, and low dielectric loss at room temperature. $BaTiO_3$ is lead-free (non-toxic) ferroelectric material and so it is environmentally friendly which makes it a more suitable material for various applications [7].

$BaTiO_3$ possesses four crystal structures at specific temperature called Curie temperature (transition temperature). Out of four the one (cubic) structure is paraelectric phase of $BaTiO_3$. The rest of the three (tetragonal, orthorhombic, and rhombohedral) structures are in ferroelectric phase as shown in the figure.

At Curie temperature T_c the material goes through a transition from *paraelectric* (PE) to a *ferroelectric* (FE) phase. The structure symmetry of ferroelectric is lower than the corresponding paraelectric structure. At $T > T_c$ the crystal does not show ferroelectricity, although for $T < T_c$ it is ferroelectric. In the case of more than one ferroelectric phase (e.g., in $BaTiO_3$) as shown in figure 1:11, the temperature upon which the ferroelectric crystal transforms from one phase to another is called the transition temperature.

1.9.1 Structure Properties of BTO

Barium titanate (BaTiO3) is a perovskite-type oxide ceramic material with a cubic crystal structure. It has a lattice parameter of about 4.01 Å and a density of about 6.35 g/cm3. The crystal structure of barium titanate is composed of a three-dimensional network of titanium and oxygen atoms, with barium ions located in the interstitial sites. Barium titanate has a high melting point of around 2200°C and is a good electrical insulator at room temperature. However, it exhibits a ferroelectric phase transition at a temperature of about 120°C, which means that it can exhibit spontaneous polarization below this temperature [23]. This property is related to the displacement of the barium ions within the lattice and gives rise to the high dielectric constant of the material. Barium titanate is also a piezoelectric material, which means that it exhibits a strain in response to an applied electric field and vice versa. This property is related to the symmetry of the crystal structure and allows barium titanate to be used in a variety of piezoelectric devices, such as sensors, actuators, and transducers. In addition to its piezoelectric and ferroelectric

properties, barium titanate is also a good dielectric, with a high dielectric constant and excellent dielectric strength. It is also chemically stable and has a good temperature coefficient of capacitance. These properties make barium titanate a widely used material in a variety of electronic and electrical applications. The dielectric constant of $BaTiO_3$ (BTO) ferroelectric crystal show variations with temperature as it cools down from its paraelectric (non-ferroelectric) cubic phase to the ferroelectric tetragonal, orthorhombic, and rhombohedral phases figure 1:13. Near the phase transition temperatures, thermodynamic properties containing dielectric, elastic, optical, and thermal constants show anomalous behavior. This is due to a distortion in the crystal as the phase changes.

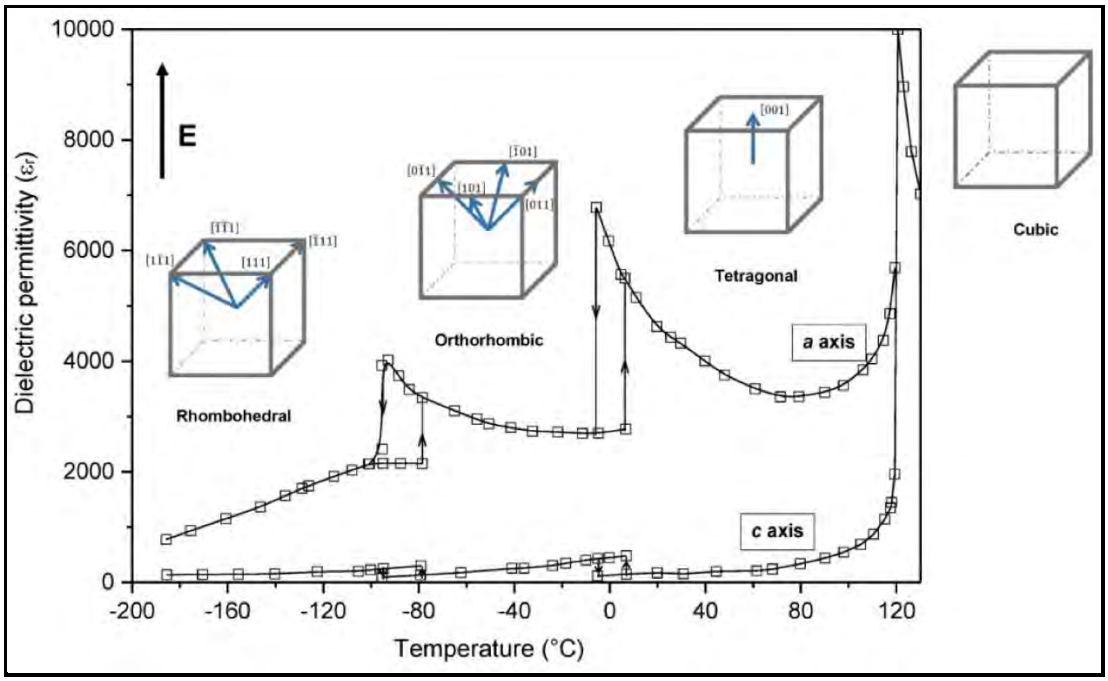

Figure 1:13: Phase transition of BTO dielectric permitivity with temperature [24].

1.9.2 Dielectric Properties of BTO

Barium titanate (BaTiO3) is a ceramic material with high dielectric constant and excellent dielectric strength. It has a high Curie temperature, good chemical stability, and good temperature coefficient of capacitance [23]. The dielectric constant of barium titanate is relatively high, ranging from around 1000 to over 4000, depending on the composition, temperature, and frequency of the applied electric field. The dielectric loss of barium titanate is

also relatively low, typically less than 0.1 at low frequencies and increasing at higher frequencies. The dielectric constant and loss of barium titanate can be affected by several factors, including temperature, humidity, and the presence of impurities or defects in the material. Barium titanate is also sensitive to mechanical stress, which can affect its dielectric properties. Overall, barium titanate is considered to have good dielectric properties and is widely used in a variety of electronic and electrical applications, including capacitors, piezoelectric devices, and high-frequency filters.

1.9.3 Ferroelectric Properties of BTO

Barium titanate ($BaTiO_3$) is a ferroelectric material that exhibits a ferroelectric phase transition at a temperature of about 120°C. Below this temperature, barium titanate exhibits spontaneous polarization, which is related to the displacement of the barium ions within the crystal lattice. The ferroelectric properties of barium titanate are influenced by several factors, including temperature, pressure, and the presence of impurities or defects in the material. The ferroelectric behavior of barium titanate can be characterized by several parameters, including the Curie temperature, the dielectric constant, and the polarization. The Curie temperature of barium titanate is the temperature at which the material loses its ferroelectric properties and becomes a paraelectric material. The Curie temperature of barium titanate is relatively high, around 120°C [25], which makes it a stable ferroelectric material over a wide temperature range. The polarization of barium titanate is related to the magnitude of the electric dipole moment per unit volume and can be measured using techniques such as pyroelectric current measurement or ferroelectric hysteresis loop measurement. Overall, the ferroelectric properties of barium titanate make it a widely used material in a variety of electronic and electrical applications, including capacitors, piezoelectric devices, and high-frequency filters.

1.9.4 BTO Thin Films

BTO thin films are like super thin layers of a special material called Barium Titanate. These thin films have properties related to electricity, light, and movement, which makes them helpful in lots of electronic and optical stuff. To make BTO thin films, we use different methods, like lasers, vapors, or chemicals, to put the Barium Titanate on a surface, which we call the substrate. Each method has its benefits, and it helps us control how the thin film will turn out, like how thick it is or how rough the surface looks. We can use BTO thin films in many devices,

such as capacitors (for storing electric charge), sensors (for sensing things around us), and actuators (for making things move). The special properties of BTO thin films also make them great for non-volatile memories (like long-term storage) and optical waveguides (to guide light). In electronics, BTO thin films are good for making dynamic random-access memory (DRAM) capacitors because they can switch their properties, helping us store lots of data in a small space. And since they can convert pressure into electricity, we can use them in sensors and actuators too. In the world of optics (light stuff), BTO thin films are super useful in structures called waveguides, where we can change how light moves through them by using electricity. This lets us create cool things like optical switches and devices that can control light. Overall, BTO thin films are flexible and can be used in all sorts of electronic, light-related, and tiny mechanical systems. They help us make advanced technologies that are used in many areas of our lives.

1.10 Literature Review of BTO films prepared by PLD

Several research studies have investigated the growth and properties of BTO films prepared by PLD. A study by Liu et al. (2014) reported the growth of BTO films on different substrates such as SrTiO3, LaAlO3, and Si using PLD [26]. The authors investigated the effect of deposition temperature and oxygen pressure on the structural, morphological, and electrical properties of the films. They found that the BTO films grown at a temperature of 700 °C and an oxygen pressure of 10 mTorr exhibited the best structural and electrical properties.

Another study by Lu et al. (2015) reported the growth of BTO thin films on SrRuO3/SrTiO3 substrates using PLD [27]. The authors investigated the effect of oxygen pressure on the structural and magnetic properties of films. They found that increasing the oxygen pressure during deposition resulted in a higher degree of epitaxy and improved magnetic properties of the films.

In a study by Koo et al. (2017), BTO thin films were prepared on different substrates such as SrRuO3/SrTiO3, LaNiO3/SrTiO3, and La0.7Sr0.3MnO3/SrTiO3 using PLD [28]. The authors investigated the effect of substrate-induced strain on the ferroelectric and magnetic properties of the films. They found that the strain induced by the substrate had a significant impact on the ferroelectric and magnetic properties of the BTO films.

In a more recent study, Hu et al. (2020) reported the growth of BTO thin films on Si substrates using PLD [29]. The authors investigated the effect of substrate temperature on the

structural and electrical properties of the films. They found that the BTO films grown at a substrate temperature of 650 °C exhibited the best structural and electrical properties.

Overall, the literature suggests that PLD is a promising method for the preparation of high-quality BTO thin films with tunable structural, electrical, and magnetic properties. The properties of the films can be optimized by controlling the deposition parameters such as deposition temperature, oxygen pressure, and substrate-induced strain.

1.11 Critical Issues of BaTiO3

Barium titanate (BaTiO3) is a ceramic material that is used in many electronic devices because it has some really good properties, like being able to store electric charge and convert pressure into electricity. However, there are some problems with barium titanate that can affect how well it works in certain situations. One issue is that it is sensitive to mechanical stress [30]. When it's put under pressure, its special properties can change, and this can be a problem in some applications. Another problem is that it's hard to make high-quality barium titanate with a consistent structure and without any defects or impurities. This can affect how well it performs, especially in cases where we need it to be very pure and consistent.

Lastly, barium titanate is not very strong. It can break easily, and this can be a problem in applications where we need it to be tough and long-lasting. To fix these issues, we need to choose the right type of barium titanate for each application and use advanced techniques to make it better. By doing this, we can improve its performance and make it more reliable for different uses.

1.12 Application of Ferroelectrics

Ferroelectric materials are super useful in many different areas like electronics, optics, and energy storage. Let me tell you about some common applications of these special materials:

1.12.1 Capacitors

Ferroelectric materials are used as a dielectric to form a capacitor out of it which is used in phones, computers etc. A schematic diagram of the ferroelectric capacitor is shown in figure 1:14.

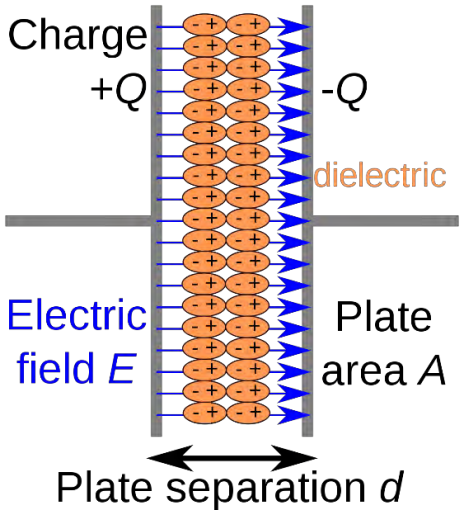

Figure 1:14: diagram of ferroelectric capacitors [31].

1.12.1 Non-volatile memory

Ferroelectric materials have another important application in non-volatile memory devices. These are special memory devices that can keep data even when we turn off the power. Two examples of such devices are ferroelectric random access memory (FeRAM) and ferroelectric tunnel junctions (FTJs). In FeRAM, the ferroelectric material is used to store data in a way that remains stable even without electricity. It's like having a tiny magnet inside the memory cell that remembers its state even when the power goes off. This makes FeRAM very fast and efficient for storing and retrieving data. In FTJs, ferroelectric materials are used in combination with other materials to create memory cells. These cells work based on the tunneling of electrons through the ferroelectric material. Just like FeRAM, FTJs also retain data without electricity, making them valuable in certain memory applications.

1.12.3 Piezoelectric transducers

Ferroelectric materials are special because they can do something cool called "piezoelectricity." This means they can change mechanical energy (like pressure or vibrations) into electrical energy, and also turn electrical energy back into mechanical energy. Because of this ability, we use them in different devices called "transducers." These transducers are used in things like ultrasound machines (to see inside the body), pressure sensors (to measure pressure in

different things), and vibration sensors (to detect vibrations or movements). So, ferroelectric materials are very helpful in making these devices work well. A schematic diagram of the ferroelectric transducers is shown in figure 1:15.

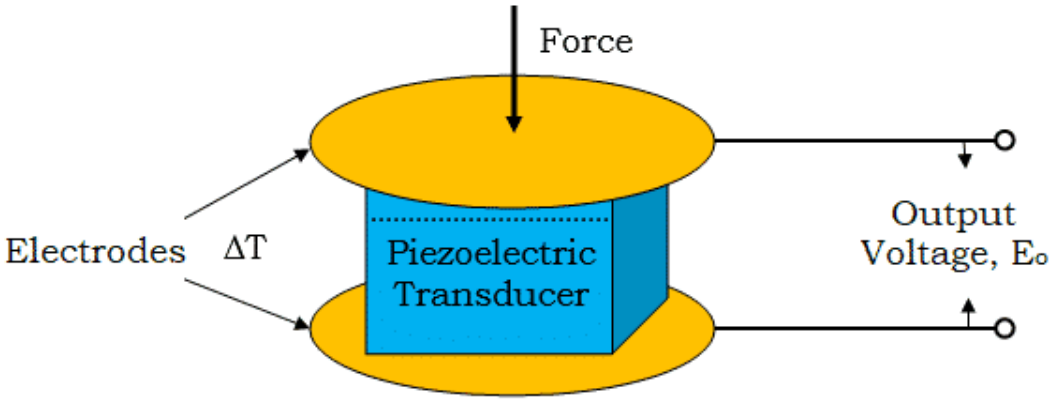

Figure 1:15: principle of ferroelectric transducers [32].

1.12.4 Electro-optic devices

Ferroelectric materials also have electro-optic properties, which means they can change the polarization of light passing through them in response to an applied electric field. This makes them useful in devices such as modulators, switches, and optical filters.

1.12.5 Energy storage

Ferroelectric materials are excellent for storing energy in different devices, like capacitors and batteries. This is because they have a special property called "high dielectric constant." This means they can hold a lot of electric charge. In capacitors, ferroelectric materials help store and release electric charge efficiently, making them essential in many electronic circuits. They are like tiny rechargeable batteries that can quickly store and release energy when needed.
Similarly, in certain types of batteries, ferroelectric materials play a role in holding and releasing electric charge. This helps the batteries work efficiently and have good performance in various applications. Overall, ferroelectric materials are essential in energy storage devices because of their ability to hold a large amount of charge, making them useful in many electronic and energy-related technologies.

1.13 Motivation

BTO (Barium Titanate) is a special material that has some really useful properties. When we make it into thin layers, we call it BTO thin film. These thin films are used in many different electronic and mechanical devices because of their unique abilities. One of the cool things about BTO thin films is that they have a high dielectric constant [33]. This means they can store and hold a lot of electric charge, which is essential for many electronic components. They also have piezoelectric properties [34], which means they can convert mechanical stress or pressure into electrical signals. This feature is very helpful in making sensors and actuators [35], which are devices that sense things in the environment or cause movement. Another great aspect of BTO thin films is that we can control their properties by adjusting how we make them. For example, by changing the temperature, pressure, or the material we put BTO on (the substrate), we can make it behave differently. This makes it very versatile and suitable for a wide range of applications. When we use BTO thin films in devices, they tend to work well for a long time without any issues. This stability and reliability make them excellent for long-term use in various electronic and mechanical systems [36]. Furthermore, BTO thin films can easily work together with other materials. This compatibility is essential when we need to integrate BTO into complex devices with different components [37]. It allows us to create more advanced and efficient systems.

In summary, we use BTO as a thin film because it has many properties, like its ability to store charge and convert pressure into electrical signals. These properties can be adjusted to fit specific needs, and BTO thin films are stable and reliable for long-term use. Also, they can easily work with other materials, making them suitable for many different electronic and mechanical applications.

Chapter-2 Experimental Techniques and Characterizations

2.1 Introduction

This chapter discusses all the experimental methodologies and experimental setups that were used in the current research work. This chapter also includes a detailed description of the synthesis of pure BTO thin films. All the experimental techniques used for the synthesis and characterization used for pure BTO thin films are discussed below.

2.2 Synthesis Equipment

2.2.1 Sonicator

In thin films fabrication, the first step is to properly clean the substrates on which thin films have to grow. For that purpose, a Sonicator is used. There are three steps for substrate cleaning. First, the substrates were cleaned in Isopropanol. Substrates were placed in a beaker having Isopropanol and dipped with the tip of the Sonicator. Sound waves with a frequency range of 20kHz have been applied for 10 minutes. After that, the process repeats by placing the substrates in hellmanex. And at last, the substrates were sonicated in deionized water for 10 minutes. These sound vibrations are helpful in removing the contaminants that are sticking with substrates. This process is known as ultra-sonication. A schematic diagram of the Sonicator is shown in figure 2.1.

Figure 2.1: Sonicator for substrate washing.

2.2.2 Hydraulic Press and Die

A manual hydraulic press with a 13mm pellet press die is used for the formation of pellets. In a hydraulic press, a hydraulic cylinder is used for compressive force. The principle of the hydraulic press is based on Pascal's law. Pascal's law says that pressure applied to a fluid confined in a cylinder will be transferred equally in magnitude to every part of the liquid and to the walls of the container. A hydraulic press and pellet press die are shown in figure 2.2. Pallets are formed under the force of 7tons force for 10 min with the help of hydraulic presser.

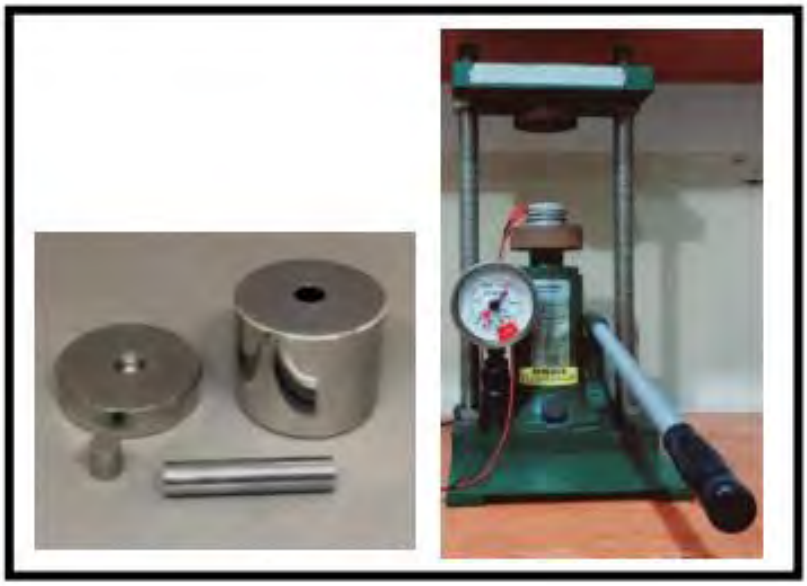

Figure 2.2: Hydraulic presser for pallet formation.

A piston in a hydraulic press works like a pump, which delivers a mechanical force to the sample region. A larger mechanical power is generated using the piston having a larger area.

2.2.3 Tube Furnace

All pallets that were formed with hydraulic presser were annealed in the tube furnace to harden these pallets. Temperatures up to 1000°C can be handled by this device. In the tube furnace, all of the prepared Pallet's samples were annealed at 900°C for 3 hours. The tube furnace used for that purpose is shown in figure 2.3.

Figure 2.3: Tube furnace [38].

2.3 Techniques for synthesis of thin films

There are many techniques by which thin films can be synthesis, some of them are as follow:

2.3.1 RF sputtering

The RF sputtering technique and the biasing in it along with the chamber insight is shown in figure 2.4. In RF sputtering technique, the target is supplied with an AC power source containing Radio frequency wavelength. During the positive cycle of the AC source applied to the target, a large electronic current flow through it while in the negative cycle, a small ionic current flow through it. It is because the electrons are very less resistible to the periodic change of the AC source as compared to ions. So, there is a net negative biasing on the target. One of the advantages of using an RF source is that the AC signals can be coupled through the impedance [39]. In this case, the electrodes can be insulator, dielectrics, or conductors. The restriction of using conductor as target is no longer there.

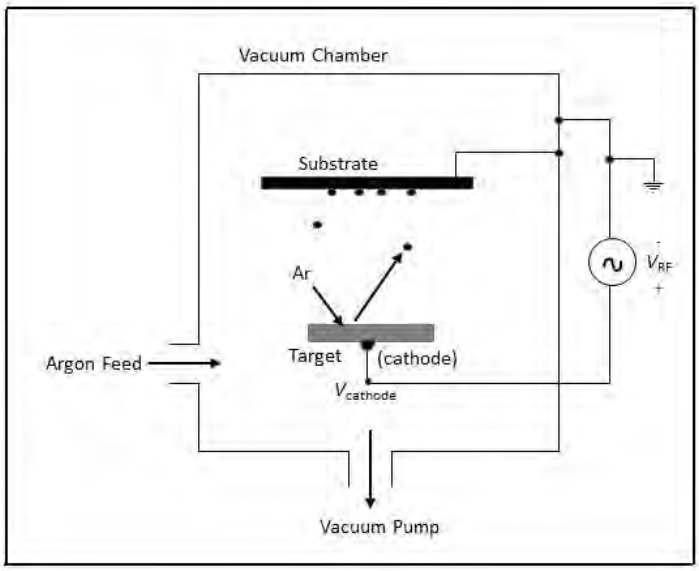

Figure 2.4: Schematic diagram of RF sputtering.

2.3.2 Pulse Laser Deposition

Another powerful and efficient Physical Vapor Deposition technique which we have used in our research is the Pulsed Laser Deposition (PLD) technique. In which a highly energetic laser beam is being shined on target material to vaporize it. These vapors are then deposited on substrate that makes a thin film. The whole process takes place in a vacuum chamber. Target material, energy of the laser beam, distance from target to substrate and the pressure of gas in the vacuum chamber are some crucial factors which determine the deposition rate of thin film on substrate. Usually, the whole process occurs in ultra-high vacuum with small amount of background gas in vacuum chamber like argon and oxygen.

The process of thin film formation by PLD can be divided into four steps:

1. Ablation of target material by laser shining.
2. Dynamics of plasma plume of ablated target material.
3. Deposition of target material on substrate.
4. Nucleation and thin film growth on substrate.

The software used for PLD is the same i.e., Neocera Pulsed Energy Deposition System. Each of these steps plays a vital role in determining the stoichiometry, uniformity, and crystallinity of the thin film.

2.3.2.1 Ablation of target material by laser shining

We employed Nd: YAG(Neodymium doped Yttrium Aluminum Garnet) pulsed laser system to ablate the material, this laser from Quintel. The laser head of the system is shown in figure. A xenon or krypton flash lamp is used to pump it, producing a laser beam with a wavelength of 1064*nm*. By employing the second and third harmonics, one may also create laser beams with wavelengths of 532*nm* and 355*nm*, correspondingly. Here 355*nm* pulsed laser used in this work as shown in figure 2.5. The irradiation of laser on target material and the removal of atoms from the surface of target material via vaporization is a complex non-linear phenomenon. When the laser is shined on the target material, it penetrates the surface of the target material. Penetration depth depends on the index of refraction of the target material and the wavelength of the laser light. The electric field of the laser light causes the free electrons of the material to oscillate. These oscillating electrons collide with the atoms of target material near the surface. These collisions heat up the surface and thus result in vaporization of atoms from the surface of target material.

Figure 2.5: Diagram of Nd: YAG pulsed Laser.

2.3.2.2 Dynamics of plasma plumes of ablated target material

The plasma plumes of target material formed due to vaporization of the material by laser irradiation follow Gaussian distribution i.e., there is a range of kinetic energies of these evaporated particles. These vapors are directed toward substrate as shown in schematic figure 2.6. It is also noted that the high energy particles can re-sputter the deposited thin film on substrate. By increasing background pressure, the high energetic species in the plasma plume can be slowed down.

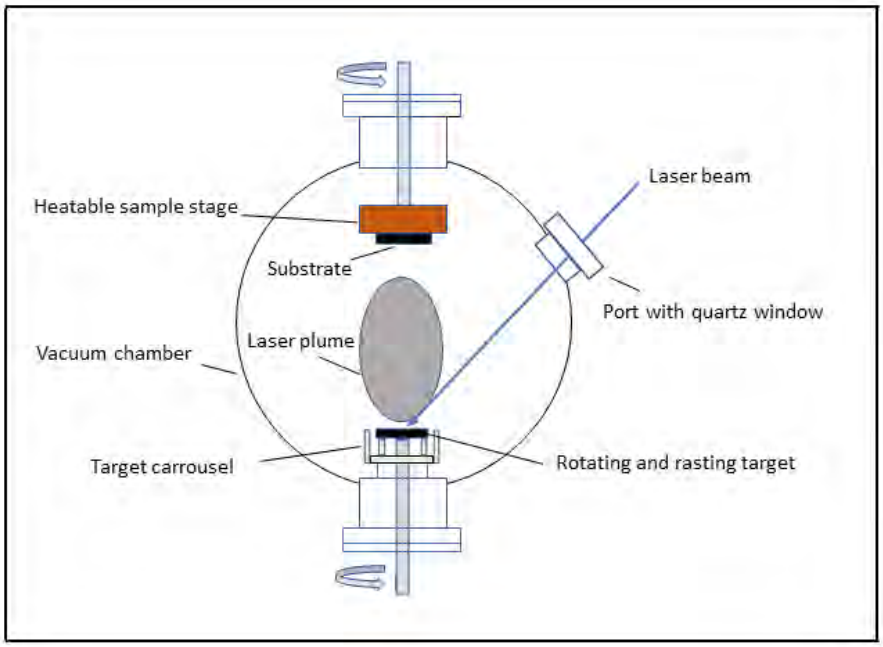

Figure 2.6: Schematic diagram of PLD System.

2.3.2.3 Deposition of target material on substrate

Due to bombardment of high energy species in plasma plume of vaporized target material on the deposited film on substrate, the atoms are sputtered off from the film. These sputtered atoms and the high energy species in plasma plume form a collision region. For condensation of particles this collision region serves as a source. A thermal equilibrium is reached when the condensation rate is high. And thin film starts growing on the surface of substrate.

2.3.2.4 Nucleation and thin film growth on substrate

There are several parameters which directly affect the nucleation process and the growth of thin film on the surface of substrate which includes the energy of laser beam, degree of ionization of target material, the flux of deposition, temperature of the surface, surface of the substrate and the pressure of background gases. The smoothness of the film is increased by large nucleation density.

2.3.3 Chemical Vapor Deposition

Most of the time, atoms from the vapor phase are used in thin film growth procedures. The main differences between various techniques are that there are various methods for producing precursor vapors such as heat-based vaporization known as evaporation, highly energetically particles-based vaporization known as sputtering, and even sometimes feeding the reactant in a gaseous state in a chamber, where these gases made the desired compound on the substrate by chemical reaction known as CVD [40]. The schematic diagram of the process that are used in growth of 2-D materials are show in figure 2.7.

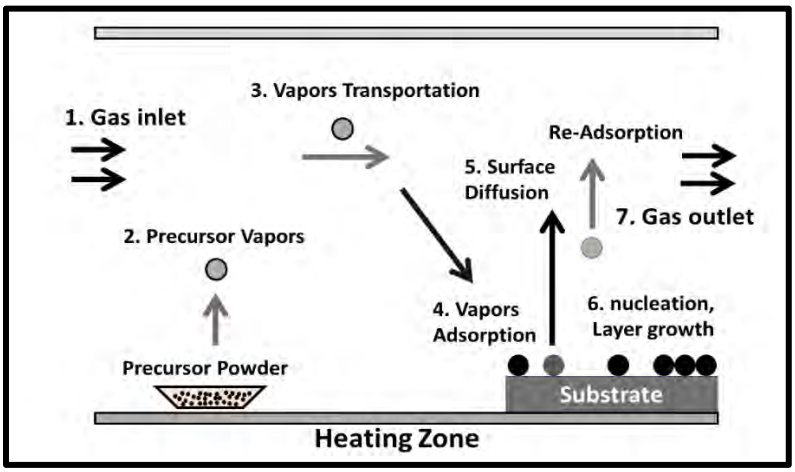

Figure 2.7: Schematic of processes involve in growth of 2D materials in CVD system.

2.4 Characterizations Techniques

Material characterization refers to the process of studying and analyzing the properties, composition, structure, and behavior of materials. It involves various techniques and methods to understand the physical, chemical, mechanical, thermal, electrical, and optical properties of different materials. Material characterization is crucial in fields such as materials science, engineering, manufacturing, and research and development. Here are some common techniques used for material characterization:

2.4.1 XRD (X-ray diffraction)

The X-ray Diffractometer shown in figure 2.8 was used to determine the phase of polycrystalline material. Additionally, it indicates the unit cell's dimensions. The X-ray

Diffractometer is a device that allows for the easy determination of crystal structure, crystal defects, interplanar spacing distance, and grain size based on the diffraction pattern.

Figure 2.8: XRD Setup.

2.4.1.1 Working Principle

The XRD technique is based on Bragg's law.

$$2dsin\theta=n\lambda$$

Where d denotes the distance between atomic planes, θ is the angle of incidence, n denotes a positive integer, and λ denotes the X-Ray wavelength. Cathode ray tubes were used to generate these X-rays, which were subsequently filtered to produce monochromatic radiation. This law establishes a relationship between the wavelength of electromagnetic radiation to the lattice spacing and diffraction angle. On the crystal surface, an incident beam of parallel X-rays is reflected off the parallel atomic planes as shown in Figure 2.9. Depending on the path difference between the reflected X-rays, the reflected X-rays will interfere constructively or destructively. When the path difference is an integral multiple of the X-ray wavelength, constructive interference occurs, resulting in the formation of a distinctive diffraction pattern. After

comparing the recorded diffraction pattern to a known database of reference patterns, the crystal structure of the material can be determined.

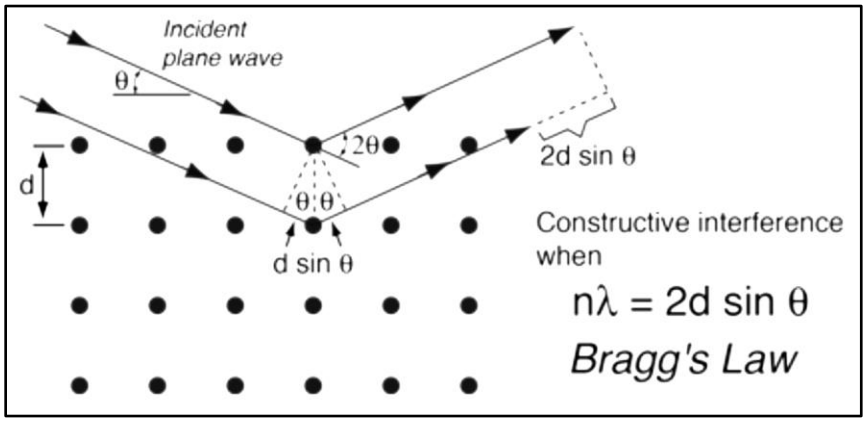

Figure 2.9: X-ray diffraction from lattice planes.

2.4.1.2 Structural Investigation

The measurement is made using a PANalytical Empyrean system diffractometer. The operating voltage and current were 40 kV and 40 mA, respectively. Copper was used as an X-ray source with a characteristic wavelength of *Kα1~ 1.540593 Å*, *Kα2 ~ 1.54442 Å* and K_β *~ 1.54187 Å*. The sample is laid out on a flat glass slide, which is then sandwiched between the detector and the X-Ray source. X-rays are incident on the target material, and the reflected rays in the shape of a pattern are recorded. This data ranges from 20º to 80º with 0.02º increments and a 2 sec stay time. XRD analysis was performed using Bragg Brentano geometry. The instrument comes with a fixed set of divergence slits. These fixed divergence slits must be put into slots on the Prefix module. There is an X-ray source, a sample stage, and a detector in a powder X-ray diffractometer as shown in figure 2.10.

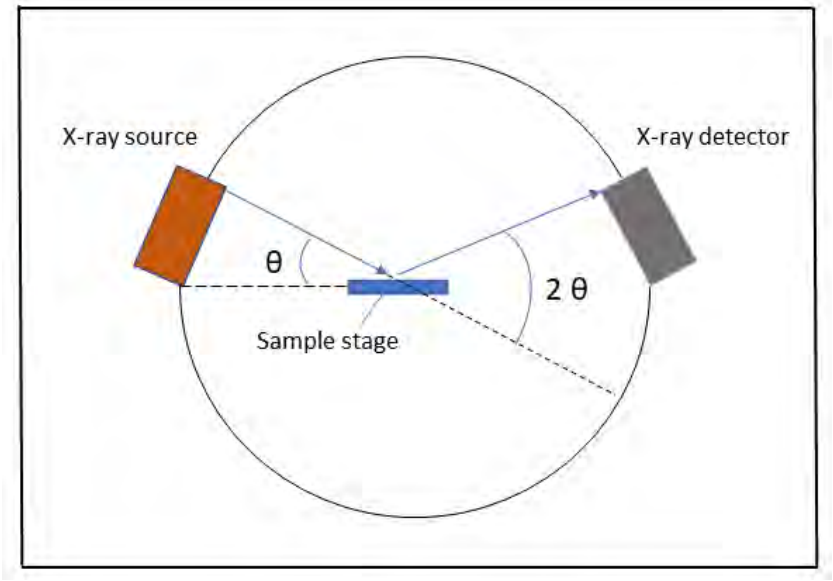

Figure 2.10: Schematic diagram of X-ray diffraction.

2.4.2 SEM (Scanning Electron Microscope)

A scanning electron microscope (SEM) is a very suitable way that is extensively used for studying the surface of materials down to the nm level. SEM is typically utilized when the desired resolution is greater than 1000x, which is the best resolution of available optical microscope. According to de Broglie every particle has a wave nature associated with it, and the liner momentum of the particle is inversely proportional to the corresponding wavelength. Electrons have a smaller wavelength than photons in the visible spectrum, so they are utilized as the incidence source for higher resolution of the SEM. A high energy beam of an electrons (0.2–40 keV) is focused on the surface of sample to produce the SEM image. The sample's surface emitted secondary electrons and other signals like X-rays that revealed details about the material composition and surface topography. Figure 2.11 shows a schematic of SEM system. The primary operational components of the SEM system are the electron gun, condenser lenses, scanning coils, high vacuum sample chamber, secondary electron detectors, and computer for image processing.

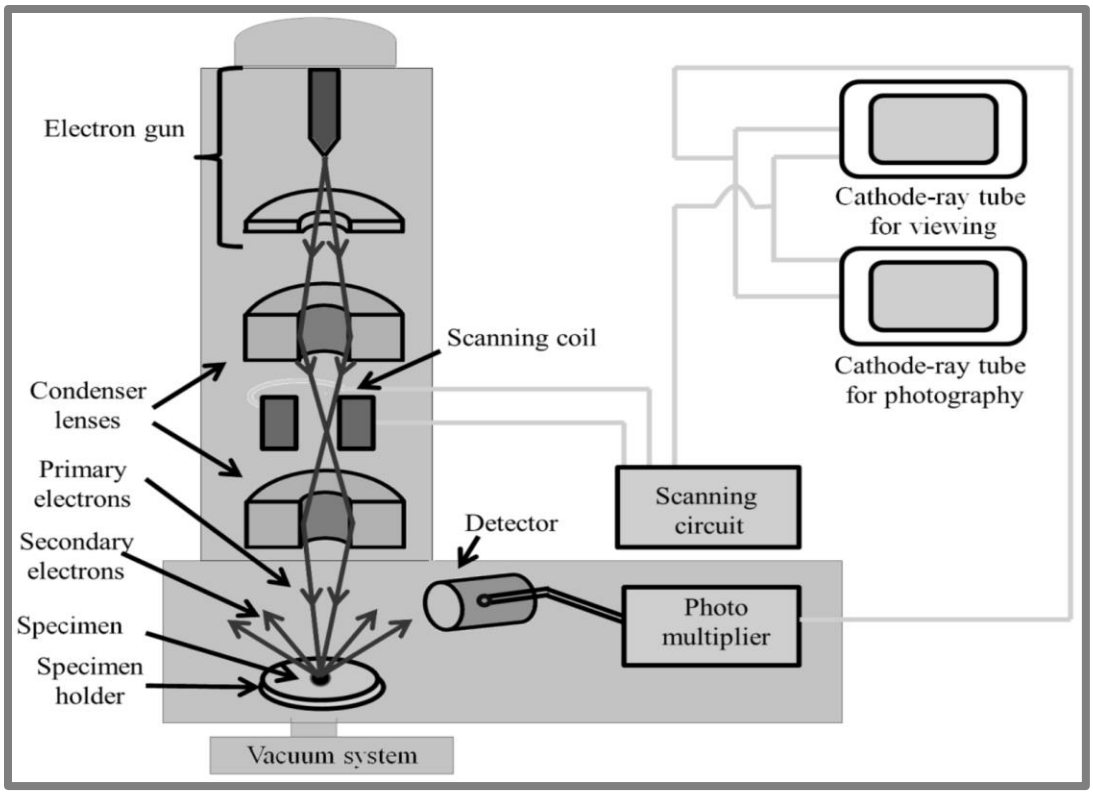

Figure 2.11: Schematic diagram of SEM [41].

The thermionic emission and electrodes are used to produce high energy electron emissions from the electron gun situated at the top of the system. Tungsten filament is a typical material used for high-energy electron emission. The electrons are then transmitted through a tiny disc (condenser aperture) with a hole of micron size that controls the diameter of the electron beam. The appropriate-diameter electron beam was then transmitted through a number of electromagnetic lenses, commonly referred to as condenser lenses. By adjusting the condenser lenses' strength, the electron beams focus can be adjusted. After making the coarse adjustment, the fine adjustment can be made without disturbing the lenses magnification. The electrons then passed from scanning coils that adjust the electron beam position on sample. Additionally, the beam can scan across the sample surface thanks to these coils. The interaction between the electron beam and the sample surface after it has passed via the objective lens results in a variety of signals, including secondary electrons, backscattered electrons, x-rays, and photons, all of which can be detected by the appropriate detectors. Secondary electrons are picked up for SEM

measurements, and energy-dispersive x-ray spectroscopy (EDX), which analyses the sample's composition, uses x-ray signals. The SEM system used here is shown in figure 2.12.

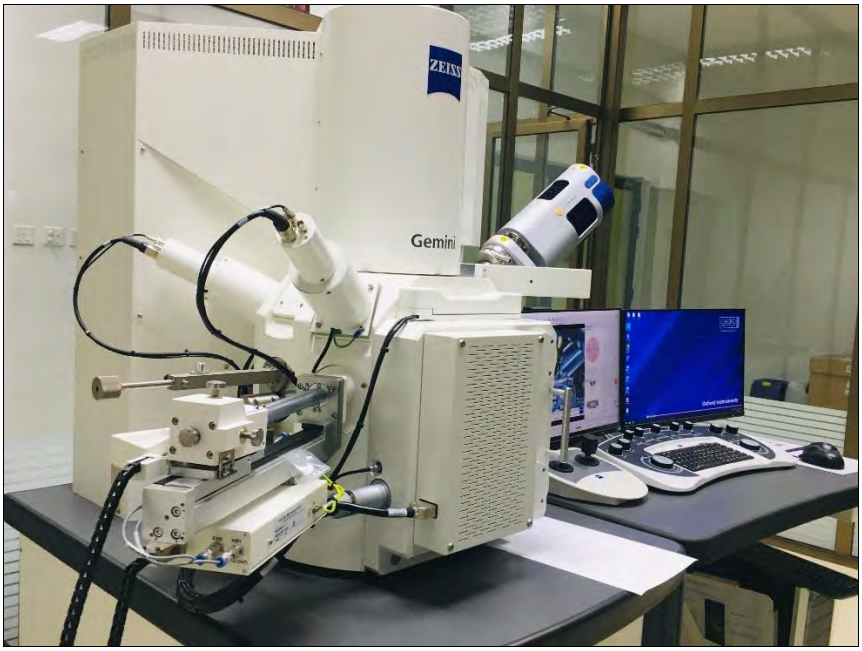

Figure 2.12: SEM System.

2.4.3 Atomic force microscope (AFM)

Atomic force microscopy (AFM) is the most popular technique for studying surface topography in 3D at the nanoscale. After the development of STM in the early 1980s, it is invented by Garber and Bin in 1986 [42]. It is mostly used to measure layer thickness in two-dimensional material characterization. The AFM probe is commonly composed of silicon or silicon nitride and has a diameter of less than 10 nm and a length of a few microns.

The vertical chip, which typically has lateral dimensions of 100 to 200 um, ends with a sharp tip. The cantilever deflected or bent when it was brought close to the sample surface due to the electrostatic force created between tip and the surface. As the AFM tip scans the sample surface, the four-quadrant optical detector measures the cantilever's deflection. Many forces may have contributed to the cantilever's deflection during the tip-sample interaction. The most prominent and common force associated with the AFM process is an interatomic force commonly referred to as the van der Waals force.

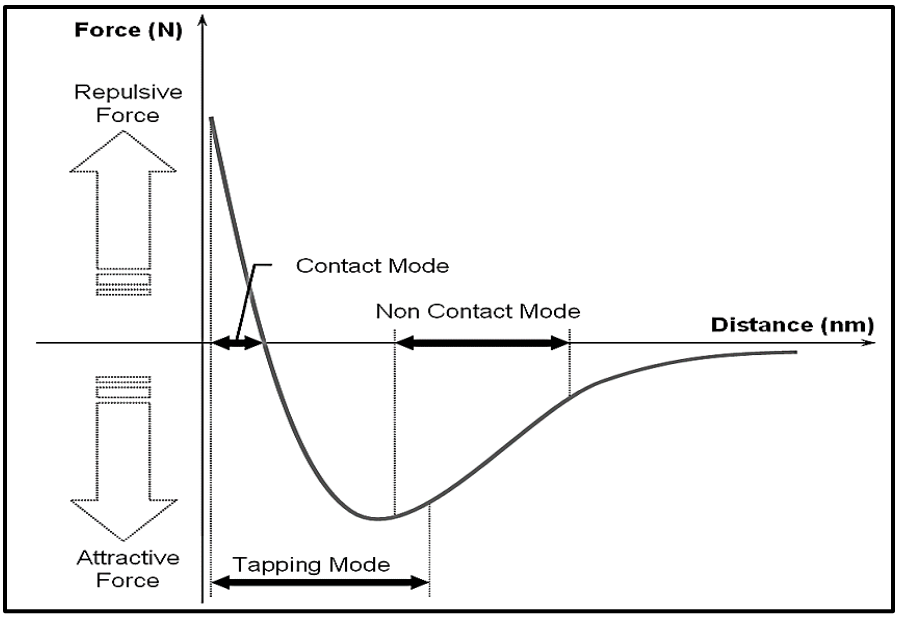

Figure 2.13: Diagram showing the interatomic force in response to distance between tip and the surface of sample. Three AFM modes' operating regions are also demonstrated.

Figure 2.13 Diagram showing the interatomic force in response to distance between tip and the surface of sample. Three AFM modes' operating regions are also demonstrated. Figure 2.13 shows the relationship between the tip-sample distance and the van der Waals force strength. When the distance is shorter, the interaction force is greater, and as the distance increases, it gradually decreases. The force vs. distance curve is typically separated into three zones, which serve as the basis for three AFM modes. The AFM mode known as contact mode, in which it operates at the smaller distance zone. The distance between the sample and the tip in the contact mode is smaller than a few angstroms and has repulsive force between them. The tip-to-sample distance in the non-contact mode is 1–10 nm, and the forces are attractive (because of the long-range van der Waals forces). The AFM contact mode is suitable for soft materials with little roughness or a smooth surface [43]. The tapping mode is the third one, in which tip vibrates up and down with frequency and change in frequency due to thickness variation of sample give rise a contrast [44].

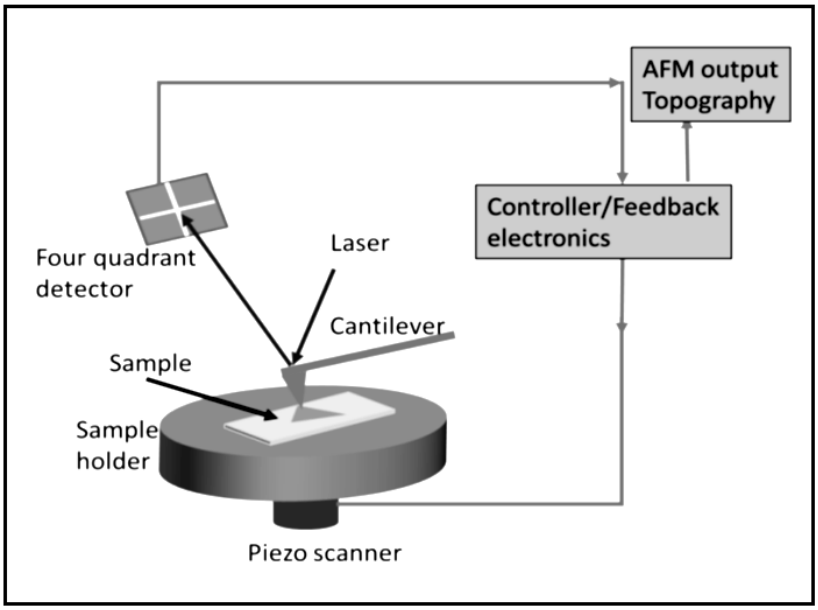

Figure 2.14: Schematic diagram of basic AFM.

Figure 2.14 illustrates the basic AFM system's schematic. In which the sample is positioned on the piezo sensor's top-mounted holder. To track the cantilever bending during the scanning, a laser with a 632 nm wavelength is mounted to the top of the cantilever. The laser deflection is recorded optically using a four-quadrant photodiode. To prevent tip damage, a feedback loop is also utilized to maintain specific sample-tip distance during scanning by setting a certain value as a setpoint.

2.5 Optical measurements

Numerous techniques are available for measuring the spectral properties of various substances. The spectrometer is a widely used tool for determining the wavelengths of optical spectra, such as transmittance, reflectance, and absorption. The spectroradiometer is used to determine spectral emission. We use a photo spectrometer for optical investigations because the band gap and its variation can be easily determined from reflection spectra.

2.5.1 UV-Visible spectrometer

To determine the optical properties, we used the Lambda 950, a flexible double beam spectrometer capable of functioning in the ultraviolet and visible spectrum ranges. Additionally,

it operates in the near infrared region. It comprises a 160mm diameter integrating sphere. Double beam and double monochromator are used to eliminate the background signal present during measurements. Deuterium and halogen lamps are the most often used light sources since they cover the whole UV range. Photomultiplier tubes and PbS detectors are used to detect in the UV-visible and near-infrared ranges, respectively. A wide wavelength range of 175nm to 3300nm is covered by this instrument, which has a resolution of ≤ 5nm. The optical components are coated with silica for long-term durability [45]. The Lambda 950 spectrometer is illustrated in Figure 2.15.

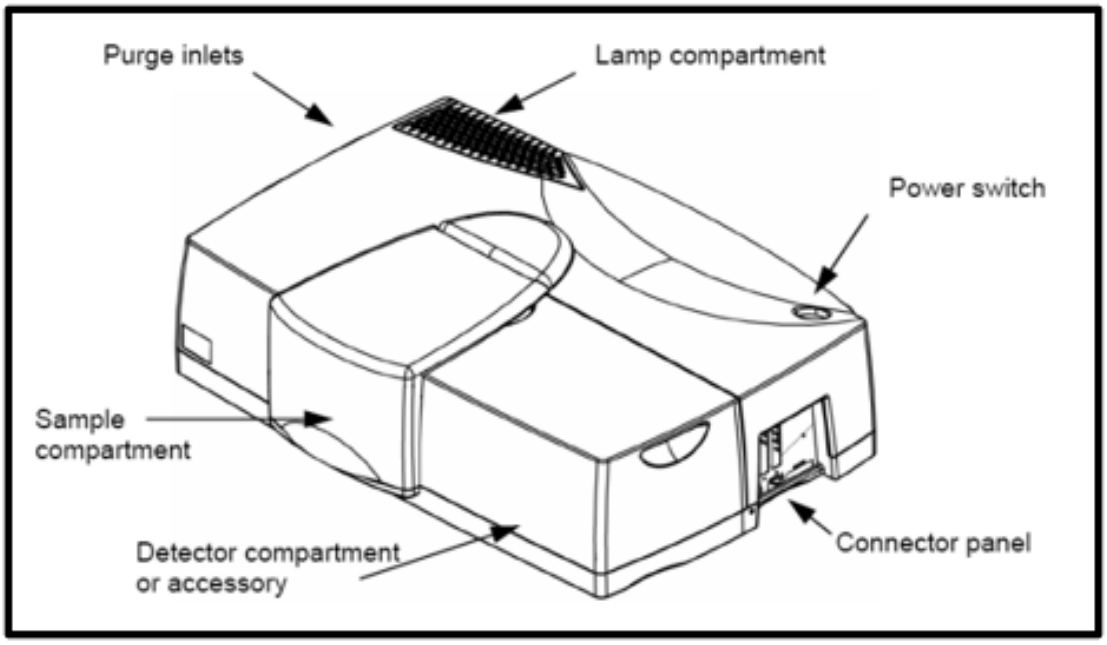

Figure 2.15: UV-vis spectroscopy setup.

Four windows are included in the spectrometer. All optical compartments of the spectrometer are sealed. Similarly, the sample compartment is sealed using a window between the detector component and the optical compartment. The silica windows that seal the sample chamber assist protect the instrument's optics from dust and gases. The sample's chemical composition and concentration can be determined from the spectrum, which is a graphic depiction of the sample's reflectance at various wavelengths.

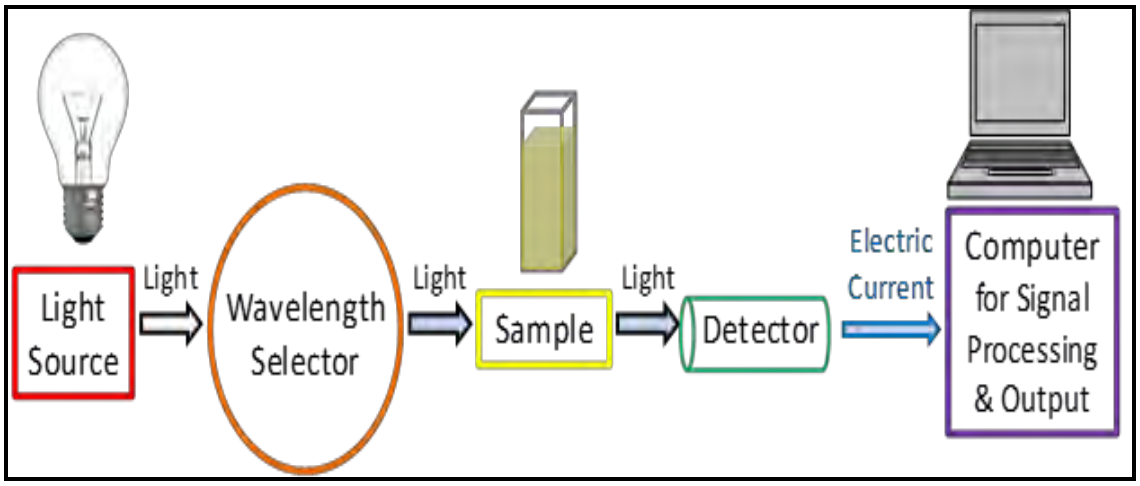

Figure 2.16: Schematic diagram of UV-vis spectrometer.

Figure 2.16 shows the schematic diagram of UV-vis spectrometer which shows how UV-vis spectroscopy works.

Chapter-3 Processing and Optimization of Thin Films synthesis.

3.1 Introduction

The synthesis of high quality and large area 2D nanostructure (graphene and TMDs etc.) has a key role in the wide range application of these materials. The synthesis techniques of 2D nanostructured materials can be generally classified into physical vapor deposition (PVD) such as molecular beam epitaxy (MBE) and pulsed laser deposition (PLD), chemical vapor deposition (CVD), and mechanical exfoliation. Here we have briefly described the mechanical exfoliation, PLD and sputtering techniques that are employed in the current experimental work.

3.2 Pulsed Laser Deposition (PLD)

3.2.1 Preparation procedure of PLD Samples

PLD setup is run with help of software, the deposition conditions for samples are given through it in a sequence. First pellet of the sample is formed with the help of hydraulic presser, placed on the plate, and mounted on the sample holder inside the chamber. The chamber is then vacuumed with the help of two vacuum pumps i.e., simple vacuum pump and rotary pump, and the pressure is reduced to few micro torr. As the vacuum is reached to the desired condition, the rotation of the pump is reduced to fill the chamber with required reactive gas up to the required pressure. Then the laser is turned on. The laser pulses hit the pallet surface of samples and ablate the target material and get deposited on the substrate above the target. There were five thin film samples prepared through PLD technique named SRO(Strontium Ruthenium Oxide) [46], BTO (Barium Titanate) at on different temperatures i.e, 700˚C, 750˚C, 800˚C, and 850˚C. The deposition conditions and parameters and their structural analysis by XRD are given below.

3.2.2 Steps for the sample preparation

Figure 3.1 shows the setup which is used in this work. There are many steps which are used to prepare the samples, some of the main steps are the following.

1. Substrate washing with isopropanol, hellmanex and deionized water.

2. Sample pasted on circular plate with the help of double tape, and then place that circular plate in chamber on sample holder trey.
3. The chamber is being vacuumed and pressure of the chamber is down to few micro torr.
4. All the parameters i.e., heater, rotation of samples and substrates, vacuum pumps, and shutters were handled with the help of computer software.
5. The heater is activated, when the temperature reaches the desired temperature then the laser ablation is started.
6. After the time for ablation is completed, then the substrate is cooled and brought back to room temperature.

Figure 3.1: PLD System [47].

Electrodes are critical components of ferroelectric thin film devices, since they allow for the measurement of electrical properties and real device functioning. SrRuO3 (SRO) was grown as electrode and the BaTiO3 (BTO) was grown as ferroelectric thin film with the help of PLD. A schematic representation of the electrode setup that was used in this work is shown in figure 3.2.

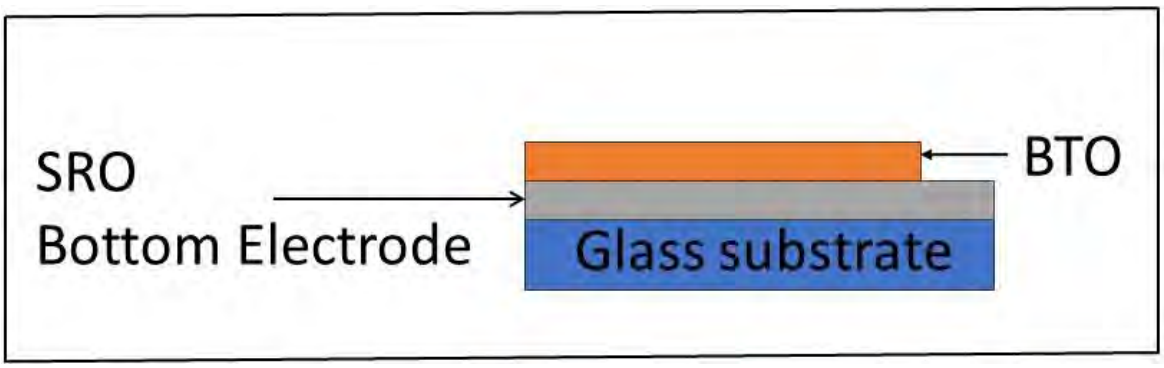

figure 3.2 Schematic representation of BTO thin film.

3.2.3 Target preparation for PLD

The target for PLD was already prepared and no commercial targets were used. BaTiO3 and SrRuO3 powder were pressed in 10cm diameter Cu cups under 7 Tons of pressure for 10 minutes and then placed in Tube Furnace under 900 °C for 2 hours. Then the pressed targets were placed in 5th and 3rd position among target placement inside the chamber respectively. The target is shown in figure 3.3.

Figure 3.3: Target used in PLD.

3.2.4 Substrate Cleaning

Substrate cleaning process were followed by the following steps:

1. The silicon substrate was cut into 10*10mm from a silicon wafer.
2. The substrate was placed in a beaker, filled with ¼ of isopropanol and then placed on a Sonicator with the frequency range of 20kHz for 10 minutes.
3. The substrate was then placed on Sonicator with the same frequency, same time, and same level of solution but in hellmanex.
4. Then the substrate was placed in deionized water for 10 minutes under the same frequency and level of deionized water.
5. And lastly, the blower was blowen to dry the substrate, and the substrate was held with the help of Tweezer.

3.3 XRD analysis of BaTiO3 powder

Powder of BaTiO3 (BTO) was already prepared and no commercially prepared samples were used. The XRD data of BTO powder is shown in figure 3.4.

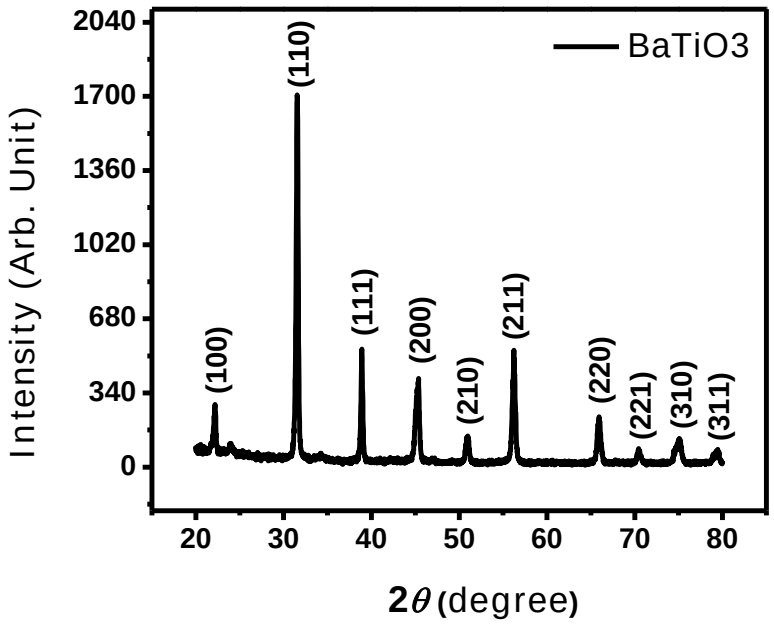

Figure 3.4: XRD spectrum of BTO powder.

The XRD analysis shows us that the peaks of BTO powder were observed at 22.214°, 31.511°, 38.900°, 45.383°, 50.993°, 56.257°, 65.896°, 70.419°, and 75.131° as shown in the figure .which shows the single phase of barium titanate (BTO) which exhibited a tetragonal phase with the space group P4mm. The analysis was performed using the reference code JCPD-01-074-2491. To confirm the identification and characterize the sample, the obtained XRD pattern was compared with the ICSD collection code 028620. As shown by the reference code above the lattice parameter and angles in unit cell of crystalline are shown in Table 3.1.

Table 3.1: Crystalline lattice parameters and angles.

Lattice parameters	a(Å)	b(Å)	c(Å)
	3.9924	3.9924	4.0309
Angles	α	β	γ
	90	90	90

3.4 XRD analysis of SrRuO3 powder

Powder of SrRuO3 (SRO) was already prepared and no commercially prepared samples were used. The XRD of BTO powder is shown in figure 3.5.

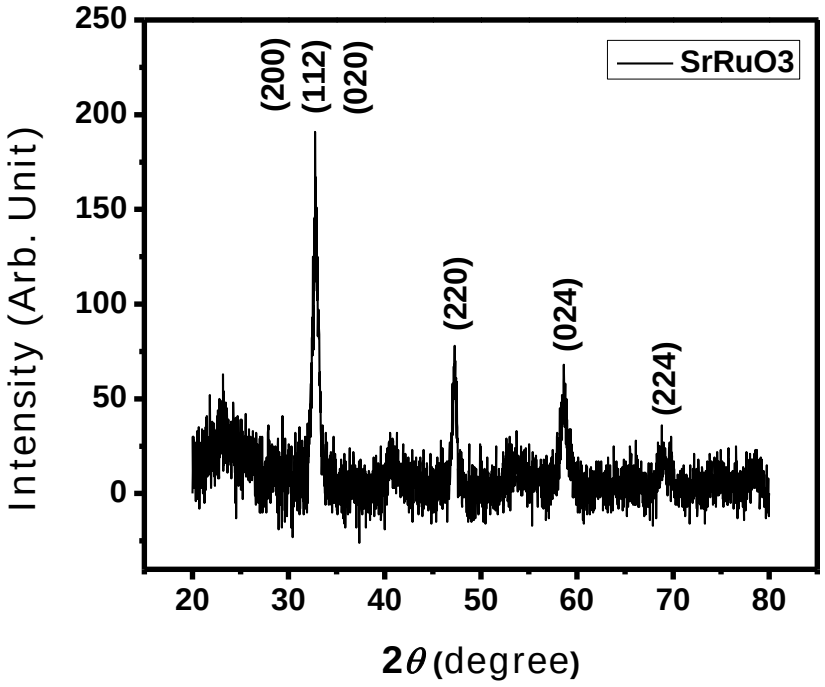

Figure 3.5: XRD spectrum of SRO powder.

The XRD analysis shows us that the peaks of SRO powder were observed at 32.812°, 47.375°, 58.646°, and 68.797° as shown in the figure .which shows the single phase of Strontium Ruthenium Oxide (SRO) which exhibited an Orthorhombic phase with the space group Pbnm. The analysis was performed using the reference code JCPD-01-079-0735. To confirm the identification and characterize the sample, the obtained XRD pattern was compared with the ICSD collection code 065691. As shown by the reference code above the lattice parameter and angles in unit cell of crystalline are shown in Table 3.2.

Table 3.2 Crystalline lattice parameters and angles.

Lattice parameters	a(Å)	b(Å)	c(Å)
	5.5670	5.5304	7.8446
Angles	α	β	γ
	90	90	90

3.5 SRO Thin Film on Si Substrate

3.5.1 Deposition conditions and parameters

All the below conditions were applied through the software controlling the PLD setup on the computer. The conditions and parameters are given in Table 3.3.

Table 3.3 Conditions and parameters for SRO thin film growth.

1	Target material	$SrRuO_3$ powder pellet of 13mm diameter
2	Distance between substrate and target	40mm
3	Base pressure	5×10^{-5} Torr
4	Temperature of substrate	775˚C
5	Reactive gas	Oxygen
6	Reactive gas pressure	2×10^{-1} Torr
7	Laser frequency	10 Hz
8	Laser ablation time	5 hours
9	Spin speed of substrate rotation	10 degrees/sec
10	Target rotation	10 degrees/sec
11	Target raster	Between 50˚ and 60˚
12	Laser wavelength	355nm
13	Annealing procedure	450˚C for 30 min under oxygen 5×10^{-1}Torr

3.5.2 Structural characterization

3.5.2.1 XRD analysis

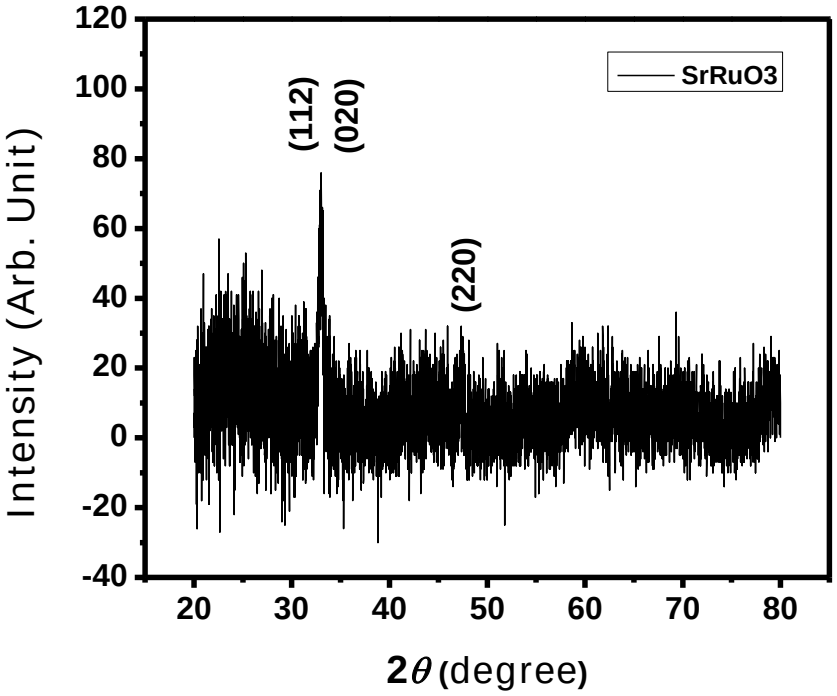

Figure 3.6: XRD spectrum of SRO thin film.

Figure 3.6 shows the XRD spectrum of SRO thin film that is grown on Si glass substrate. XRD analysis shows us that the peaks of SRO thin film were observed at 32.812°, and 47.375° as shown in the figure .which shows the single phase of Strontium Ruthenium Oxide (SRO) which exhibited an Orthorhombic phase with the space group Pbnm [48]. The analysis was performed using the reference code JCPD-01-079-0735. To confirm the identification and characterize the sample, the obtained XRD pattern was compared with the ICSD collection code 065691. As shown by the reference code above the lattice parameter and angles in unit cell of crystalline are shown in the Table 3.4

Table 3.4 Crystalline lattice parameters and angles

Lattice parameters	a(Å)	b(Å)	c(Å)
	5.5670	5.5304	7.8446
Angles	α	β	γ
	90	90	90

3.6 BTO Thin Film on Si Substrate

3.6.1 Deposition conditions and parameters

Table 3.5 Conditions and parameters for BTO thin film growth.

1	Target material	$BaTiO_3$ powder pellet of 13mm diameter
2	Distance between substrate and target	40mm
3	Base pressure	5×10^{-5} Torr
4	Temperature of substrate	800˚C
5	Reactive gas	Oxygen
6	Reactive gas pressure	9.7×10^{-2} Torr
7	Laser frequency	10 Hz
8	Laser ablation time	5 hours
9	Spin speed of substrate rotation	10 degrees/sec
10	Target rotation	10 degrees/sec
11	Target raster	Between 5˚ and 15˚

12	Laser wavelength	355nm
13	Annealing procedure	Reduce temp to 0 by 5 deg/min under 7.5 torr

3.6.2 Structural characterization

3.6.2.1 XRD analysis

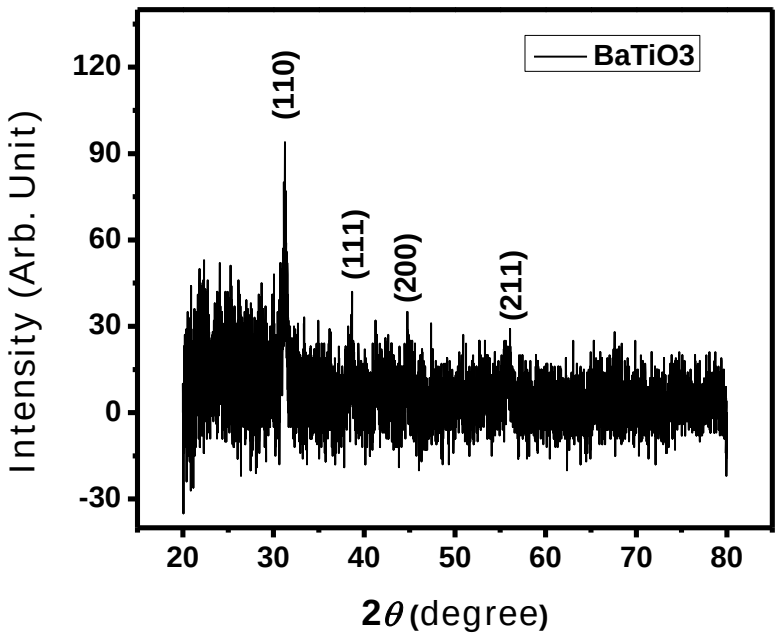

Figure 3.7: XRD spectrum of BTO thin film

Figure 3.7 shows the XRD spectrum of BTO thin film that is grown on Si glass substrate. The XRD analysis shows us that the peaks of BTO Thin film were observed at 31.511°, 38.849°, 45.164°,and 56.109° as shown in the figure .which shows the single phase of BTO which exhibited a cubic phase with the space group Pm-3m. The analysis was performed using the reference code JCPD-01-075-0461. To confirm the identification and characterize the sample, the obtained XRD pattern was compared with the ICSD collection code 029147. As shown by the reference code above the lattice parameter and angles in unit cell of crystalline are shown in the Table 3.6

Table 3.6 Crystalline lattice parameters and angles

Lattice parameters	a(Å)	b(Å)	c(Å)
	4.0119	4.0119	4.0119
Angles	α	β	γ
	90	90	90

3.7 BTO on SRO/Si Substrate

3.7.1 Deposition conditions and parameters

Table 3.7 Conditions and parameters for BTO thin film growth on SRO/Si glass substrate.

1	Target material	$BaTiO_3$ powder pellet of 13mm diameter
2	Distance between substrate and target	40mm
3	Base pressure	5×10^{-5} Torr
4	Temperature of substrate	700˚C, 750˚C, 800˚C, 850˚C
5	Reactive gas	Oxygen
6	Reactive gas pressure	9.7×10^{-2} Torr
7	Laser frequency	10 Hz
8	Laser ablation time	5 hours
9	Spin speed of substrate rotation	10 degrees/sec
10	Target rotation	10 degrees/sec
11	Target raster	Between 5˚ and 15˚

12	Laser wavelength	355nm
13	Annealing procedure	Reduce temp to 0 by 5 deg/min under 7.5 torr

3.7.2 Structural characterization

3.7.2.1 XRD analysis

Four Thin films of BTO were prepared by PLD at different temperatures i.e., 700˚C, 750˚C, 800˚C, and 850˚C on SRO/Si substrate. XRD of those four samples are given in the figure 3.8 below.

Figure 3.8: XRD spectrum of BTO thin film on SRO/Si glass substrate on different temperatures in degree celsius i.e, BTO-700, BTO-750, BTO-800, and BTO-850

The XRD analysis shows us that the peaks of pure BTO Thin film on SRO/Si glass substrate were observed at 33.215°, 40.885°, 47.264°,and 59.501° for BTO thin film, and 35.513˚ for SRO thin film as shown in the figure . There is a slight peak shift to the right in the XRD peaks which is due to mismatch of BTO and SRO lattice constants, which apply strain on each other and compress each other due to which peaks shift to which it is shifted to the right [49]. This peak

shift, because of SRO and BTO lattice mismatch as shown in figures, was not observed in SRO film grown on Si glass substrate individually and BTO film grown on Si glass substrate. XRD result illustrates that the crystallinity of the thin films decreases as temperatures of the films increases suggesting that BTO grown at 700˚C is more crystalline than that grown at 850˚C.

Chapter-4 Results and Discussion

As discussed in chapter 1, BaTiO3 (BTO) has been successfully exploited in many practical applications, such as, Capacitors, Non-volatile memory, Piezoelectric transducers, Electro-optic devices, Energy storage, Magnetic sensors etc. However, different applications require different characteristics of BTO to be optimized. For example, switching applications require low hysteresis and high value of resistance ratio whereas memory applications call for large hysteresis and so on. These properties may depend on the oxidation state, microstructure, grain size and surface morphology in the case of thin films. Here we investigate various properties of BTO thin films grown on different temperatures with the help of PLD.

4.1 Scanning Electron Microscope Analysis

Scanning Electron Microscope (SEM) is a well-established technique that explores the material morphology of samples in the form of powders, pellets or thin films etc. SEM images of BTO thin films that are grown on 700˚C, 750˚C, 800˚C and 850˚C were analyzed to study and compare the quality of films morphology. Our main aim is to compare the surface morphology and grain size of the films fabricated using PLD technique. The surface morphology of the four films is shown in figure 4.1. The scan area for all the films were different with different magnifications, the magnification of the samples is 10.13K X, 38.75K X 3.30K X, and 12.75K X respectively to the temperature of the films as shown in figure 4.1.

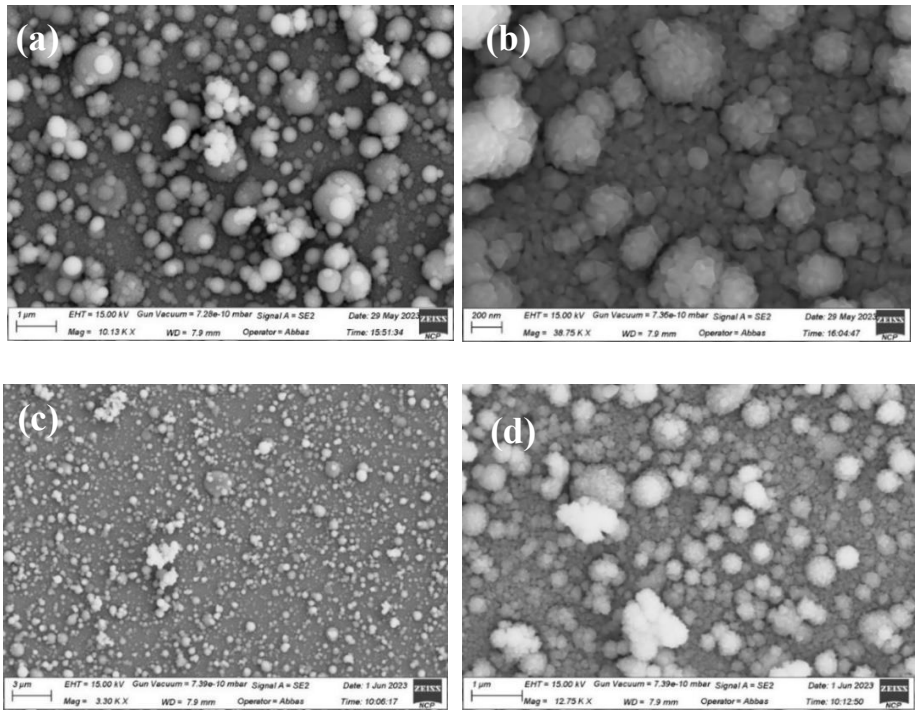

Figure 4.1: SEM images of thin films prepared on different temperature (a) 700˚C (b) 750˚C (c) 800˚C (d) 850˚C.

4.1.1 Grain Analysis

The grain analysis of four samples is done using the gauge in the image of different scales and the scales are 100 nm, 200 nm, 300 nm, and 1µm as shown in figure 4.2. The size of the grain increases as the deposition temperature increases, the average size of 700˚C thin film is 93 nm, 145 nm for 750˚C, 190 nm for 800˚C, and 245 nm for 850˚C as shown in figure while figure 4.3 shows how the size of the grain increases with temperature and it shows a linearly increasing graph [50].

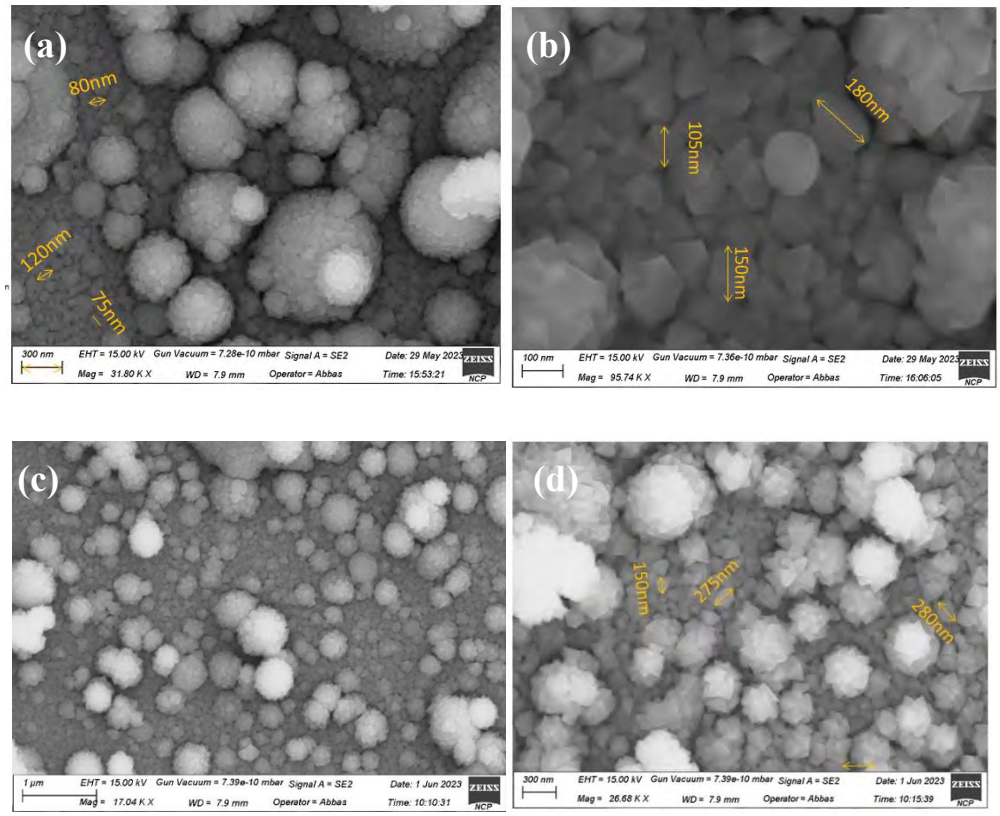

figure 4.2 Grain analysis of SEM images prepared on different temperatures (a) 700˚C (b) 750˚C (c) 800˚C (d) 850˚C.

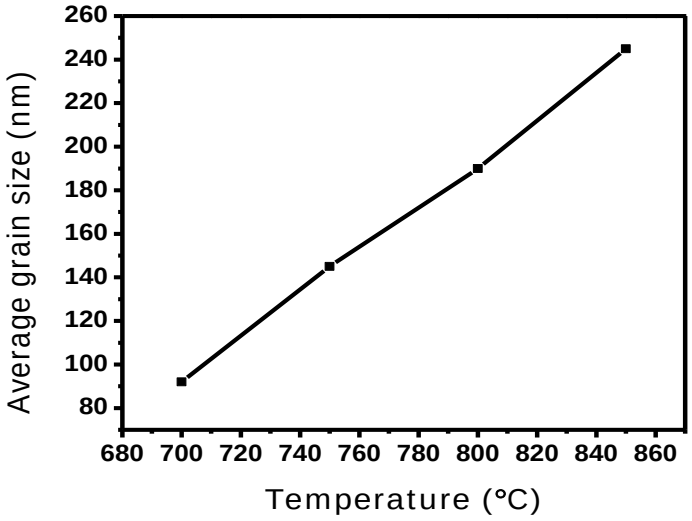

Figure 4.3 Comparison graph of thin films prepared at different temperatures; (a) 700˚C (b) 750˚C (c) 800˚C (d) 850˚C.

4.2 Atomic force Microscopic Analysis

Atomic force microscopy (AFM) is a well-established technique to explore the surface morphology of thin films. Here we have used AFM in tapping mode. A new AFM tip was used in each case, the tip used has a resonance frequency of about 335-345 kHz. AFM images of the BTO-700, BTO-750, BTO-800 and BTO-850 were analyzed to study and compare the quality of films. Our aim is to compare the roughness and Line measurement of the films prepared by PLD technique. The Line measurement and roughness of the thin film samples were obtained using the SPMlabAnalysis V7.00 software. The scan area for all the films was 5×5 μm^2. The height and phase images of BTO-700, BTO-750, BTO-800 and BTO-850 are shown in figure 4. 4. Figures 4. 5 show the scanned surface of the films in 3-D image of our four samples that how the surface morphology of these film is, from visual inspections it shows that as the temperature increases. Smoothness of the film also increases, smoothness from the visual inspection can be observed by the depth and the height of the surface of the samples [50].

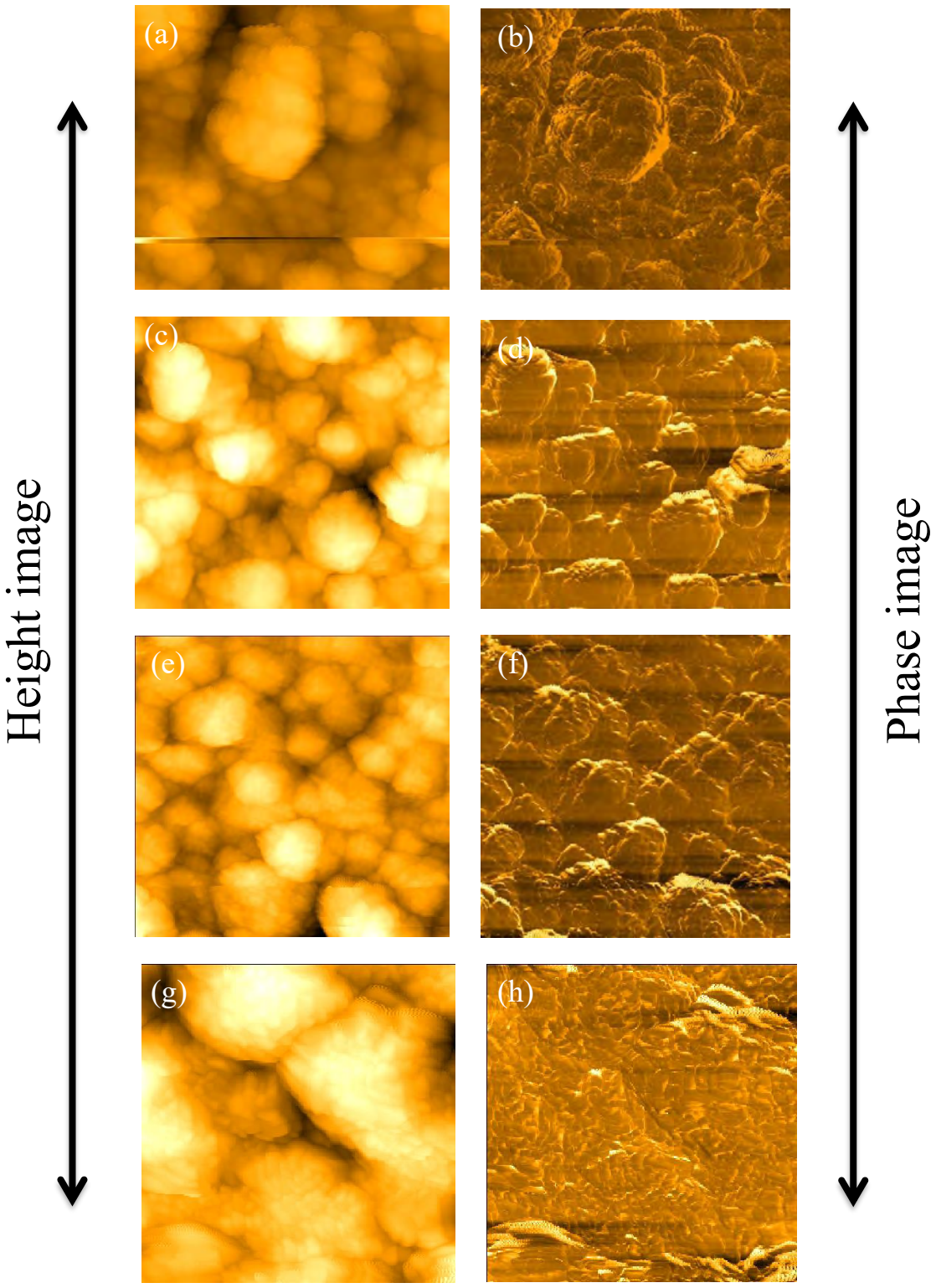

Figure 4.4: height and phase image of thin films prpared on different temperatures (a,b) 700˚C (c,d) 750˚C (e,f) 800˚C (g,h) 850˚C.

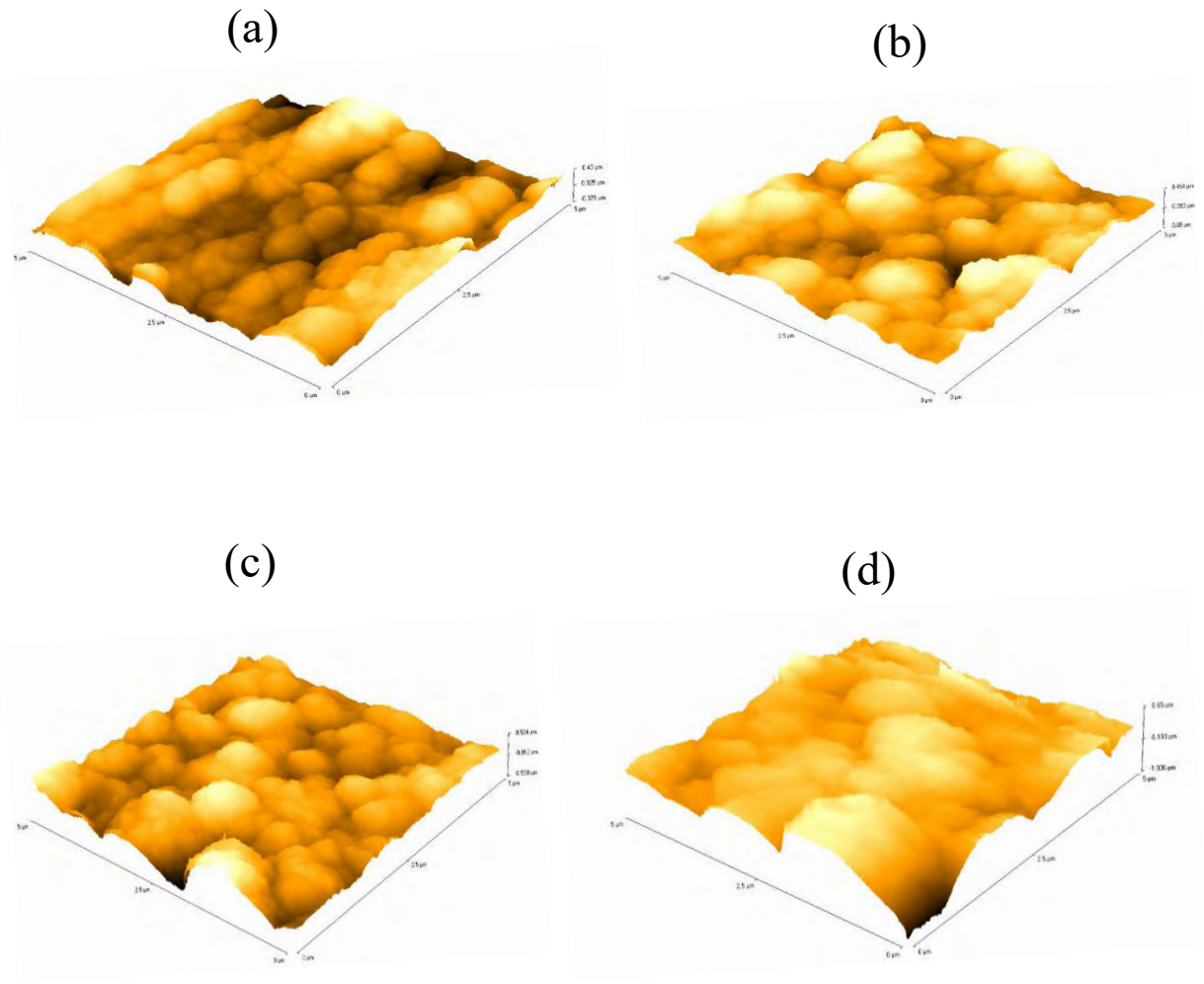

Figure 4.5: 3-D image analysis prepared at different temperatures; (a) 700˚C (b) 750˚C (c) 800˚C (d) 850˚C.

4.2.1 Roughness Analysis

Figure 4.6: Roughness Analysis of thin films prepared on different temperatures (a) 700˚C, (b) 750˚C, (c) 800˚C, (d) 850˚C.

From visual inspection the samples grown with PLD on different temperature the roughness decreases with increase in temperature. The roughness parameters of the thin film surfaces is calculated by the SPMlabAnalysis V7.00 software which are shown in figure 4.6.

We have opted for the simplest of characteristics for roughness measurement i.e., the distribution of heights and depths on the surface. Here, we have chosen two roughness parameters, average roughness R_a (the average roughness is defined as the arithmetic mean of the deviation of height from the image mean value.) and root mean square roughness RMS, (R_q, is defined as the square

root of the mean value of the squares of the distance of the points from the image mean value) of the surfaces of our samples.

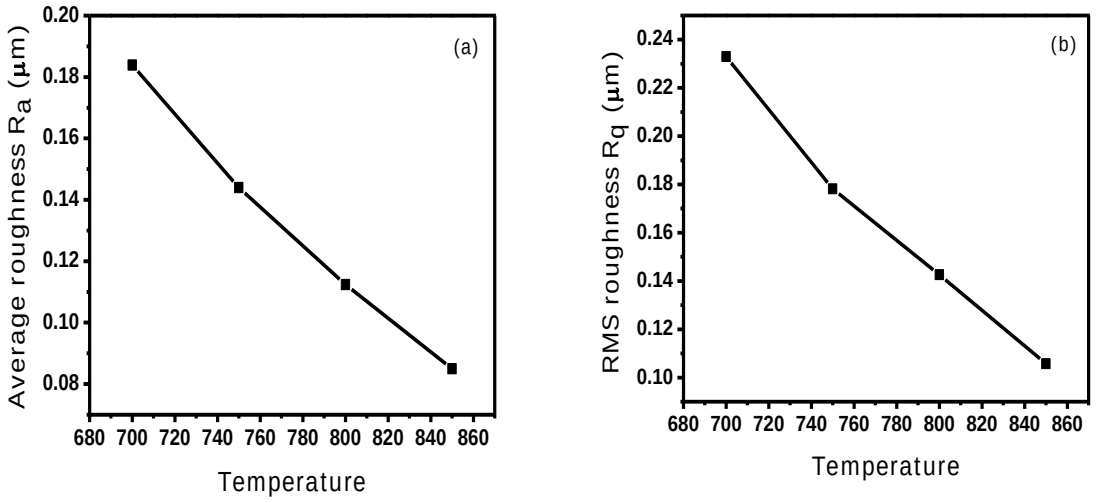

Figure 4.7: Comparison graph of; (a) Average roughness R_a and (b) Root mean square roughness of thin films prepared at temperatures 700˚C, 750˚C, 800˚C and 850˚C, respectively.

These parameters for the four samples are determined from AFM images and a comparison is shown in the tables (Figure 4.6) and plotted in term of graph shown in figure . It is evident in comparison graph (figure 4.7), that both R_a and R_q show a same trend of decrease in roughness of the films. Note that all samples were prepared through PLD procedure, which shows that roughness decreases as the deposition temperature of BTO thin films increases.

4.2.2 Line Measurement

Line Measurement is a technique of AFM data which shows how the surface of the thin film is on the respected line. The Line Measurement of the thin film surfaces prepared on different temperature i.e., 700˚C, 750˚C, 800˚C, and 850˚C is calculated by the SPMlabAnalysis V7.00 software as shown in the below figure 4.8.

From visual inspection it shows that as the temperature of the samples increases the roughness of the sample decreases, lines in the graph shows the height and depth of the samples morphology as shown in figure 4.8 on the right-sided of figure.

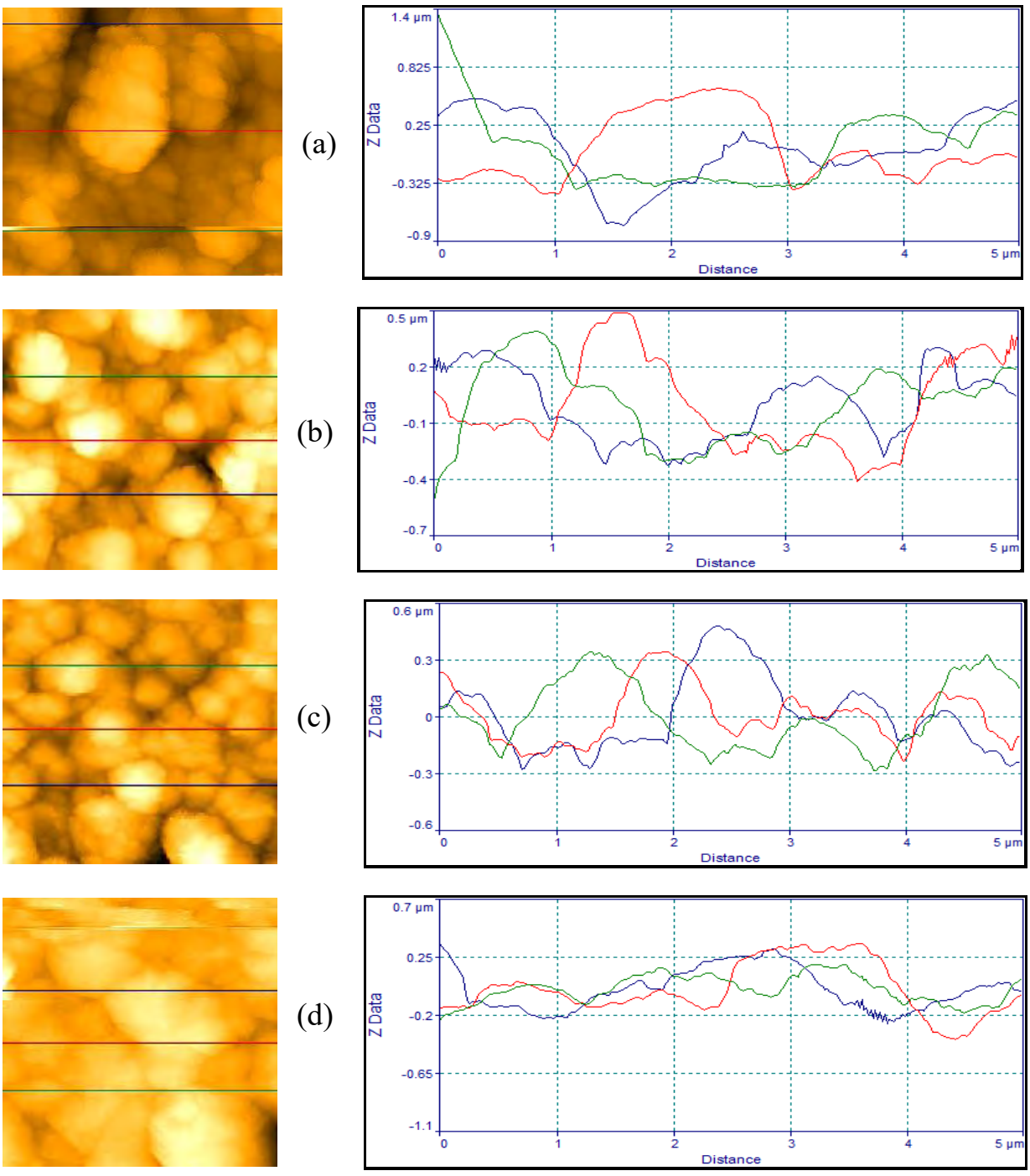

Figure 4.8: Line measurement analysis of thin films prepared on different temperatures (a) 700˚C (b) 750˚C (c) 800˚C (d) 850˚C.

4.3 UV-Vis Spectroscopy

The optical response of pure BTO thin film fabrication on different temperature will be discussed in this section.

4.3.1 Optical Measurement of pure BTO thin films

Optical characterization of pure BTO thin films were carried out at room temperature for reflectance spectroscopy. Lambda-950 Perkin-Elmer UV-Vis spectrometer was used with wavelength range of 250-850 nm and integrating sphere attachment. Figure 4.9 shows the reflectance spectra of pure BTO thin film that synthesis on different temperature i.e, 700˚C, 750˚C, 800˚C, and 850˚C.

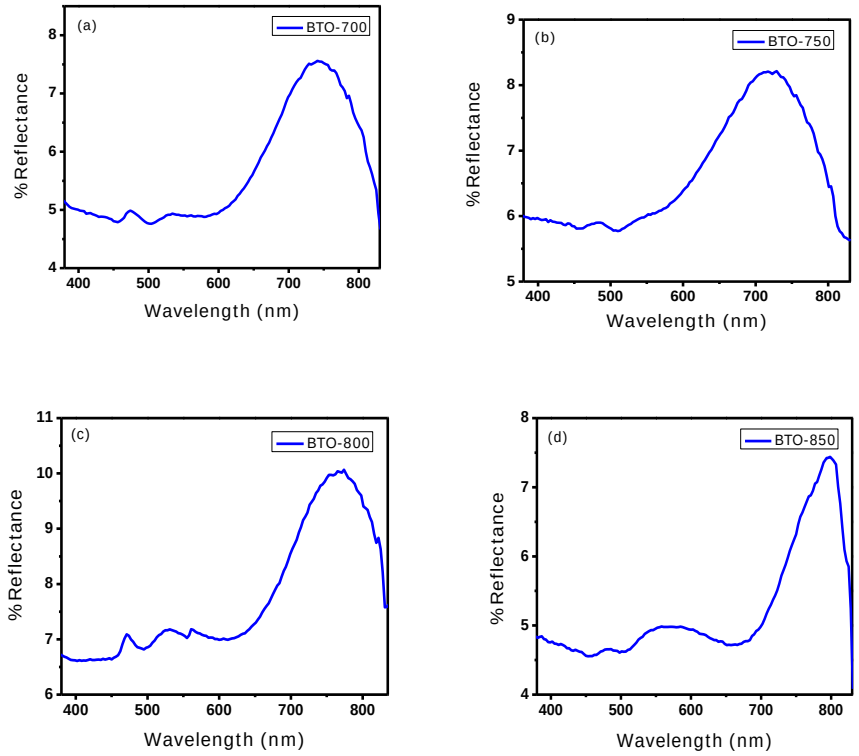

Figure 4.9: %Reflectance spectrum of BTO films prepared at different temperatures; (a) 700˚C (b) 750˚C (c) 800˚C (d) 850˚C.

4.3.2 Band Gap

The diffused reflectance spectra of BTO are indicated in figure 4.9. Where Kubelka-Munk (KM) function is $F(R) = \frac{1-R^2}{2R}$. The function $[F(R) * \mathrm{E}]^2 = [\frac{1-R^2}{2R} * \mathrm{E}]^2$ is plotted to the function of energy (E) to calculate the direct band gap. Figure 4.10 shows the band gap of the four samples prepared at different temperatures. The band gap of thin films prepared at 700˚C and 750˚C is 3.11eV, while thin films prepared at 800˚C and 850˚C have band gaps of 3.10eV and 3.07e, respectively, as shown in figure 4.10.

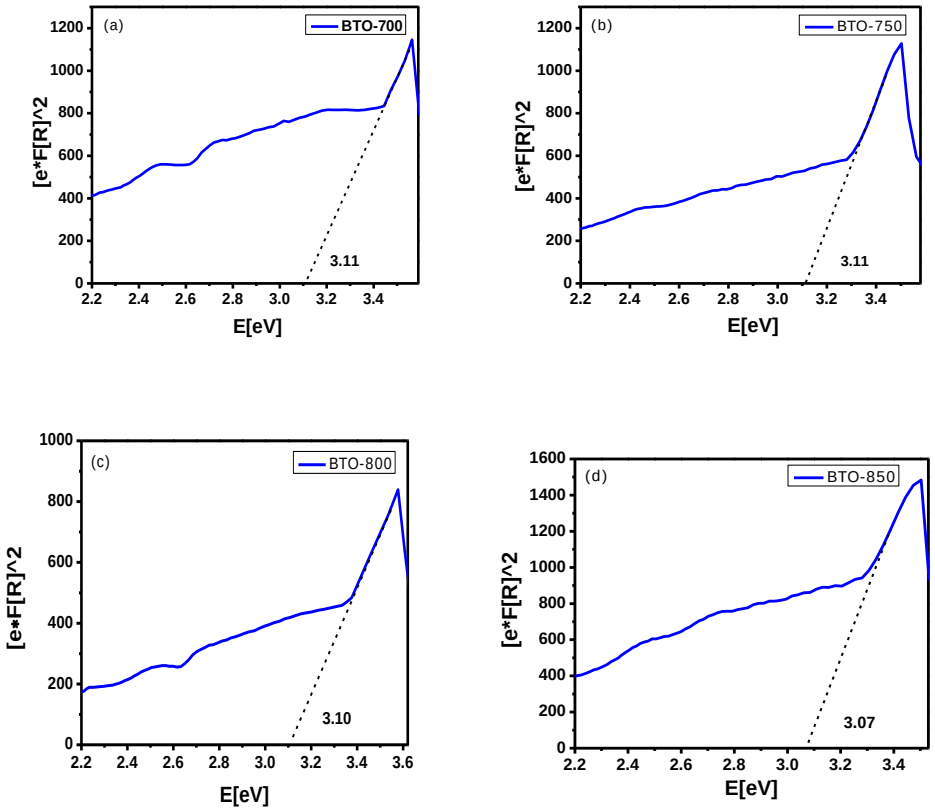

Figure 4.10: Band gaps of thin films prepared at different temperatures; (a) 700˚C (b) 750˚C (c) 800˚C and (d) 850˚C

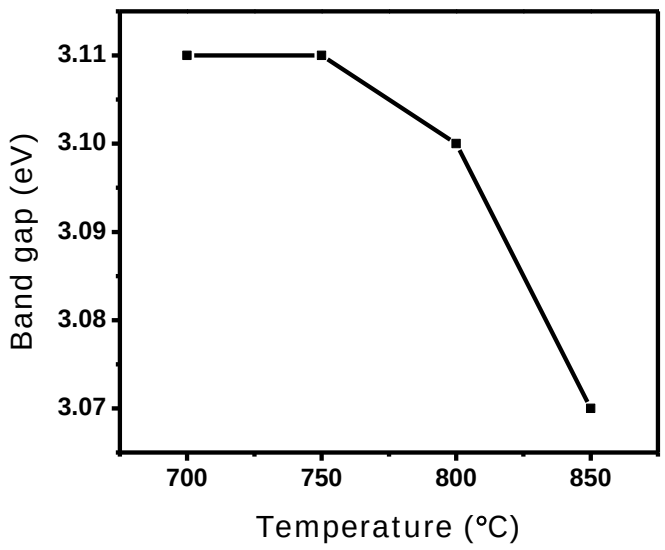

Figure 4.11: Comparison graph of Band gaps of thin films prepared at different temperatures; (a) 700˚C (b) 750˚C (c) 800˚C and (d) 850˚C.

Figure 4.11 presents comparison graph of the band gap changes with temperature, which shows that band gap decreases as the synthesis temperature of the thin films increases. The graph shows non-linear decrease in band gap with increasing synthesis temperature [50, 51].

.4.4 Conclusions

Already prepared $BaTiO_3$ (BTO) and $SrRuO_3$ (SRO) powder were used in this work, from which pellets were formed, with the help of hydraulic press, of 13mm in diameter, and these pellets were used as target in Pulsed Laser Deposition (PLD) setup. SRO thin film was just used as bottom electrode and then BTO thin films at different temperatures (700˚C, 750˚C, 800˚C, 850˚C) were grown on SRO/Si glass substrates.

XRD analysis shows that when SRO and BTO thin films grow on Si glass substrate individually, they exhibit orthorhombic and cubic phases, respectively, but when BTO grows on SRO/Si glass substrate it has a little peak shift of 1.7 degrees which is attributed to lattice mismatch of SRO

and BTO thin films due to which films apply strain on one another, and a peak shift occurs. As the synthesis temperature of the films increases the crystallinity of the films decreases.

SEM images were taken at different magnifications which show that the grain size of BTO films increases with increasing the temperature of the substrate successively.

In AFM analysis of the four samples prepared at different temperatures, the height and phase images, 3-D images, and Line measurement were analyzed which show that as the synthesis temperature of the samples increases the roughness of the films decreases, roughness can be defined as the height and depth of the sample's morphology. Visual inspection and line measurement clearly illustrate the relationship of temperature and roughness of films.

Optical properties were studied by diffused reflectance spectroscopy and direct band gap was calculated using Kubelka-Munk function which shows that as the synthesis temperature of the samples increases the band gap of the films decreases.

References

1. Zhang, F. and T. Rice, *Effective Hamiltonian for the superconducting Cu oxides.* Physical Review B, 1988. **37**(7): p. 3759.
2. Gerra, G., et al., *Ionic polarizability of conductive metal oxides and critical thickness for ferroelectricity in BaTiO 3.* Physical review letters, 2006. **96**(10): p. 107603.
3. Tomioka, Y., et al., *Collapse of a charge-ordered state under a magnetic field in Pr 1/2 Sr 1/2 MnO 3.* Physical Review Letters, 1995. **74**(25): p. 5108.
4. Taz, H., et al., *Integration of amorphous ferromagnetic oxides with multiferroic materials for room temperature magnetoelectric spintronics.* Scientific reports, 2020. **10**(1): p. 3583.
5. Chen, W., et al., *Two-dimensional Janus transition metal oxides and chalcogenides: multifunctional properties for photocatalysts, electronics, and energy conversion.* ACS applied materials & interfaces, 2018. **10**(41): p. 35289-35295.
6. Choi, W., et al., *Recent development of two-dimensional transition metal dichalcogenides and their applications.* Materials Today, 2017. **20**(3): p. 116-130.
7. Choi, K.J., et al., *Enhancement of ferroelectricity in strained BaTiO3 thin films.* Science, 2004. **306**(5698): p. 1005-1009.
8. Vandersande, J. and C. Wood, *The thermal conductivity of insulators and semiconductors.* Contemporary Physics, 1986. **27**(2): p. 117-144.
9. Krzywinski, J., et al., *Conductors, semiconductors, and insulators irradiated with short-wavelength free-electron laser.* Journal of Applied Physics, 2007. **101**(4).
10. Peiris, N., *Microwave-assisted processing of solid materials for sustainable energy related electronic and optoelectronic applications*. 2014, Loughborough University Loughborough.
11. Kao, K.C., *Dielectric phenomena in solids*. 2004: Elsevier.
12. Dalkin, T., *Conduction and polarization mechanisms and trends in dielectrics.* IEEE Electrical Insulation Magazine, 2006. **22**(5): p. 11-28.
13. Jayaram Balasubramanyam, M.L.K.S., Sujith Thomas *Lecture Notes on Engineering Physics*. 2014.
14. Sawada, A., *Theory of space-charge polarization for determining ionic constants of electrolytic solutions.* The Journal of chemical physics, 2007. **126**(22): p. 224515.
15. Dineva, P., et al., *Piezoelectric materials*. 2014: Springer.
16. Qiu, J. and H. Ji, *The application of piezoelectric materials in smart structures in China.* International Journal of Aeronautical and Space Sciences, 2010. **11**(4): p. 266-284.
17. *What is Piezoelectric Effect?* 2022 24-01-2022; Available from: https://www.circuitbread.com/ee-faq/what-is-piezoelectric-effect.
18. Iijima, K., et al., *Preparation of ferroelectric BaTiO3 thin films by activated reactive evaporation.* Applied physics letters, 1990. **56**(6): p. 527-529.
19. Wang, T., et al., *Relaxor ferroelectric BaTiO3–Bi (Mg2/3Nb1/3) O3 ceramics for energy storage application.* Journal of the American Ceramic Society, 2015. **98**(2): p. 559-566.
20. Li, Y. and L. Chen, *Temperature-strain phase diagram for BaTiO3 thin films.* Applied physics letters, 2006. **88**(7).

21. Paul, S. and D. Kumar, *Barium titanate as a ferroelectric and piezoelectric ceramics: Barium titanate as a ferroelectric and piezoelectric ceramics.* Journal of Biosphere, 2013. **2**(1): p. 55-58.
22. Kool, T.W., *Properties of perovskites and other oxides*. 2010: World Scientific.
23. Yanase, N.Y.N., et al., *Thickness dependence of ferroelectricity in heteroepitaxial BaTiO3 thin film capacitors.* Japanese journal of applied physics, 1999. **38**(9S): p. 5305.
24. Villafuerte-Castrejón, M.E., et al., *Towards lead-free piezoceramics: Facing a synthesis challenge.* Materials, 2016. **9**(1): p. 21.
25. Damodaran, A.R., et al., *Enhancement of ferroelectric Curie temperature in BaTiO3 films via strain-induced defect dipole alignment.* Advanced materials, 2014. **26**(36): p. 6341-6347.
26. Mazet, L., et al., *Structural study and ferroelectricity of epitaxial BaTiO3 films on silicon grown by molecular beam epitaxy.* Journal of Applied Physics, 2014. **116**(21).
27. Roy, S., et al., *Interface control of electronic transport across the magnetic phase transition in SrRuO3/SrTiO3 heterointerface.* Scientific reports, 2015. **5**(1): p. 15747.
28. Sun, X., *CONTROLLABLE THREE-DIMENSIONAL STRAIN, MICROSTRUCTURE, AND FUNCTIONALITIES IN SELF-ASSEMBLED NANOCOMPOSITE THIN FILMS*. 2019, Purdue University Graduate School.
29. Ogugua, S.N., O.M. Ntwaeaborwa, and H.C. Swart, *Latest development on pulsed laser deposited thin films for advanced luminescence applications.* Coatings, 2020. **10**(11): p. 1078.
30. Desu, S.B., *Influence of stresses on the properties of ferroelectric BaTiO3 thin films.* Journal of The Electrochemical Society, 1993. **140**(10): p. 2981.
31. *https://en.wikipedia.org/wiki/Dielectric*. 2023.
32. Raghvendra, N., *Transducer – Characteristics, Type, Application, Factors Influencing Choice By Nandini Raghvendra*, in *https://electricalfundablog.com/transducer-characteristics-types/*. 2023.
33. Kumazawa, H. and K. Masuda, *Fabrication of barium titanate thin films with a high dielectric constant by a sol–gel technique.* Thin solid films, 1999. **353**(1-2): p. 144-148.
34. Roberts, S., *Dielectric and piezoelectric properties of barium titanate.* Physical Review, 1947. **71**(12): p. 890.
35. Singh, M., et al., *Synthesis and characterization of perovskite barium titanate thin film and its application as LPG sensor.* Sensors and actuators b: chemical, 2017. **241**: p. 1170-1178.
36. Park, K.-I., et al., *Piezoelectric BaTiO3 thin film nanogenerator on plastic substrates.* Nano letters, 2010. **10**(12): p. 4939-4943.
37. Hu, Y.-Q., et al., *Ultrahigh Ferroelectric and Piezoelectric Properties in BiFeO3–BaTiO3 Epitaxial Films Near Morphotropic Phase Boundary.* ACS Applied Materials & Interfaces, 2022. **14**(32): p. 36825-36833.
38. *High Temperature Tube Furnace – STF 15 / TZF 15*, in *https://prolabsystems.com/wp/product/high-temperature-tube-furnace-stf-15-tzf-15/*. 2023.
39. Lu, X., et al., *The energy gap of rf-sputtered BaTiO3 thin films with different grain size.* Thin Solid Films, 1996. **274**(1-2): p. 165-168.

40. Chern, C., et al., *Epitaxial growth of BaTiO3 thin films by plasma-enhanced metalorganic chemical vapor deposition.* Applied physics letters, 1992. **60**(9): p. 1144-1146.
41. Nixon, W.C., *Scanning electron microscopy.* Microelectronics Reliability, 1965. **4**(1): p. 55-56.
42. Reimer, L., *Transmission electron microscopy: physics of image formation and microanalysis*. Vol. 36. 2013: Springer.
43. Wang, B., et al., *Mechanically induced ferroelectric switching in BaTiO3 thin films.* Acta Materialia, 2020. **193**: p. 151-162.
44. Singh, P.K. and M. Gaur, *Enhancement of β-phase of P (VDF-TrFE) 60/40 by BaTiO3 nanofiller.* Ferroelectrics, 2018. **524**(1): p. 37-43.
45. perkinElmer. *https://resources.perkinelmer.com/lab-solutions/resources/docs/BRO_Lambda950850650Americas.pdf*. 2023.
46. Niu, G., et al., *Epitaxy of BaTiO3 thin film on Si (0 0 1) using a SrTiO3 buffer layer for non-volatile memory application.* Microelectronic Engineering, 2011. **88**(7): p. 1232-1235.
47. *http://neocera.com/product-category/pld-systems/*. PLD Systems 2020.
48. Zakharov, N., et al., *Substrate temperature dependence of structure and resistivity of SrRuO3 thin films grown by pulsed laser deposition on (100) SrTiO3.* Journal of materials research, 1999. **14**(11): p. 4385-4394.
49. Bandyopadhyay, R., et al., *Application of powder X-ray diffraction in studying the compaction behavior of bulk pharmaceutical powders.* Journal of pharmaceutical sciences, 2005. **94**(11): p. 2520-2530.
50. Supasai, T., et al., *Influence of temperature annealing on optical properties of SrTiO3/BaTiO3 multilayered films on indium tin oxide.* Applied surface science, 2010. **256**(14): p. 4462-4467.
51. Mishra, V., et al., *Metastable behavior of Urbach tail states in BaTiO3 across phase transition.* arXiv preprint arXiv:1612.06756, 2016.